



Influence of Flow Configuration and Thermal Wall Boundary Conditions on Turbulence During Premixed Flame-Wall Interaction within Low Reynolds Number Boundary Layers

Umair Ahmed¹ · Nilanjan Chakraborty¹ · Markus Klein²

Received: 18 February 2023 / Accepted: 6 June 2023 / Published online: 6 July 2023
© The Author(s) 2023

Abstract

The influence of flow configuration on flame-wall interaction (FWI) of premixed flames within turbulent boundary layers has been investigated. Direct numerical simulations (DNS) of two different flow configurations for flames interacting with chemically inert isothermal and adiabatic walls in fully developed turbulent boundary layers have been performed. The first configuration is an oblique wall interaction (OWI) of a V-flame in a turbulent channel flow and the second configuration is a head-on interaction (HOI) of a planar flame in a turbulent boundary layer. These simulations are representative of stoichiometric methane-air mixture under atmospheric conditions and the non-reacting turbulence for these simulations corresponds to the friction velocity based Reynolds number of $Re_\tau = 110$. It is found that the mean wall shear stress, mean wall friction velocity and the mean velocity statistics are affected during FWI and the behaviour for these quantities varies under the different flow configurations as well as for the different thermal wall boundary conditions. The behaviour of the quenching distance and mean wall heat flux under isothermal wall conditions is found to be significantly different between the two flow configurations. The variation of the non-dimensional temperature in wall units for cases with isothermal walls suggests that the temperature in the log-layer region is significantly altered by the evolving wall heat flux in both flow configurations. Statistics of the mean Reynolds stresses and turbulence dissipation rate show that the flame significantly alters the behaviour of turbulence due to thermal expansion effects and flow configuration plays an important role.

Keywords Flame-wall interaction · Strain rate · Turbulent channel flow · Premixed turbulent combustion · V-flame

✉ Umair Ahmed
umair.ahmed@newcastle.ac.uk

Nilanjan Chakraborty
nilanjan.chakraborty@newcastle.ac.uk

Markus Klein
markus.klein@unibw.de

¹ School of Engineering, Newcastle University, Newcastle upon Tyne NE1 7RU, UK

² Department of Aerospace Engineering, University of the Bundeswehr Munich, Neubiberg, Germany

1 Introduction

Reducing greenhouse gases and the control of pollutant emissions are becoming increasingly important for the aviation, automotive and power generation industry. This has led to more compact combustor designs resulting in higher fuel efficiency and higher energy density, but this reduction in size leads to events like flame-wall interaction (FWI) within the combustion chamber (Fernandez-Pello 2002). FWI occurs in many engineering devices (e.g. spark ignition (SI) engines, gas turbines and micro-combustors), and a full understanding of these phenomena remains challenging. Understanding of near-wall turbulence in engineering problems for non-reacting flows has been the focus of an extremely abundant literature, but the fundamental understanding and treatment of near-wall turbulence for non-reacting flows is still a challenging problem and quite often the limiting factor in practical predictions. Wall-bounded flows with heat release become even more complicated during FWI events as the presence of the walls significantly influences the combustion processes and may lead to flame quenching due to wall heat losses. The flame also has a significant influence on the flow near the wall as well as on the heat flux to the wall (Clendening et al. 1981; Ezekoye et al. 1992; Popp and Baum 1997; Alshaalan and Rutland 2002). Under these conditions, the turbulence structure is altered by the presence of walls and the interaction of flame elements with walls leads to modifications of the underlying combustion processes (Alshaalan and Rutland 1998; Gruber et al. 2010). Limited information is available regarding the behaviour of turbulence and combustion processes during FWI in fully developed boundary layers and consequently there is a lack of understanding to guide the modelling effort for industrial processes.

Several numerical and experimental studies have focused on the issues related to FWI for premixed combustion in different flow regimes and configurations. In the case of laminar flows, FWI has been extensively studied both numerically (Wichman and Bruneaux 1995; Popp and Baum 1997) and experimentally (Clendening et al. 1981; Vosen et al. 1985; Jarosinski 1986; Huang et al. 1988; Ezekoye et al. 1992). Head-on quenching of premixed turbulent flames under initial isotropic turbulence was investigated using two dimensional direct numerical simulation (DNS) data by Poinso et al. (1993). Chakraborty and co-workers (Ahmed et al. 2018; Lai and Chakraborty 2016a, 2016b; Lai et al. 2017, 2018a, 2018b; Sellmann et al. 2017) further investigated this flow configuration using three-dimensional DNS data for both unity and non-unity Lewis number flames. In this flow configuration, there is no mean flow and the flame propagates towards the wall while being wrinkled by the initial isotropic turbulence and is eventually quenched in the vicinity of the cold wall. Under these conditions, turbulence decays rapidly during the FWI process and cannot be easily quantified, but these investigations still provide important physical insights into quenching distances and the influence of chemistry in FWI. The limitations of the aforementioned flow configuration related to the quantification of turbulence in FWI can be overcome by investigating fully developed turbulence in boundary layers. Such investigations were performed using DNS by Bruneaux et al. (1996, 1997) in a constant density turbulent channel flow and this work was further developed by Alshaalan and Rutland (1998, 2002) by performing a V-flame simulation in a turbulent channel-Couette flow. These investigations demonstrate that the near-wall structures have a strong influence on the flame when it is in the vicinity of the wall. In the case of FWI in turbulent boundary layers the flame is pushed towards the wall by turbulent structures leading to higher wall heat fluxes and localised flame quenching. At the same time, the vortical structures transport unburned fluid away from the wall and carry it into the burned gases, consequently

creating pockets of fresh gases in the burnt gas regions. The work on FWI within turbulent channel flows with isothermal inert walls has been extended further by Gruber et al. (2010) and Ahmed et al. (2021b, 2021d) in the case of a V-flame interacting with isothermal inert walls, and by Gruber et al. (2012, 2018), Kitano et al. (2015), Ahmed et al. (2019c, 2020, 2023) and Bailey and Richardson (2021) in the case of turbulent boundary layer flashback for hydrogen rich premixed flames. Gruber et al. (2010) used DNS data to demonstrate the alteration of the flame structure and species distribution within the flame during the progress of FWI. Ahmed et al. (2021d) focused on the evolution of the reactive scalar gradient magnitude during FWI for a V-flame in the case of both isothermal and adiabatic wall boundary conditions. This data has been utilised by Ahmed et al. (2021b) for the assessment of turbulent premixed flame models in the case of FWI. Gruber et al. (2012) used DNS data to analyse the global features of flashback of hydrogen rich premixed combustion within the boundary layer of a turbulent channel flow and demonstrated the role of Darrieus-Landau hydrodynamic instability during flashback. In a subsequent analysis Gruber et al. (2018) focussed on transient upstream flame propagation through homogeneous and fuel-stratified hydrogen-air mixtures transported in fully developed turbulent channel flows and reported a change in combustion regime for stratified mixtures as the flame approaches the wall. Bailey and Richardson (2021) analysed the effects of swirl on the flashback process for lean hydrogen-air mixture by imposing a wall-normal pressure gradient profile and developed a model for swirl effects on the flashback speed. Ahmed et al. (2019c, 2020, 2023) utilised DNS data by Kitano et al. (2015) to analyse statistical behaviours of turbulent kinetic energy transport (Ahmed et al. 2019c), displacement speed (Ahmed et al. 2020) and flame self-interaction topology (Ahmed et al. 2023) during flashback of hydrogen-rich flames within turbulent boundary layers.

Recently, FWI has also been investigated under adiabatic wall boundary conditions by Ahmed et al. (2021c, 2021d) for a V-flame in a fully developed turbulent channel flow and a turbulent boundary layer configuration and demonstrated the effects of thermal boundary condition on the behaviour of scalar gradient, scalar variance, turbulent scalar flux and scalar dissipation rate statistics (Ahmed et al. 2021c). The influence on the flame in the near wall region during FWI has also been investigated in statistically planar turbulent premixed flames impinging on an inert flat wall at different temperatures by Zhao et al. (2018a, 2018b, 2019) and the DNS data was used to develop simplified models for wall heat transfer and flame quenching distance (Zhao et al. 2018a). Zhao et al. (2019) analysed the statistics of different modes for FWI and demonstrated the effects of FWI on the relative alignments of scalar gradient with principal strain rates along with their modelling implications. The reactive scalar gradient and flame displacement speed statistics in the same configuration for different fuel Lewis numbers was analysed by Konstantinou et al. (2021), which revealed that reactive scalar statistics and flame quenching due to heat loss through the wall are significantly affected by the fuel Lewis number. The DNS findings related to the influence of the flame on turbulence and *vice versa* have been confirmed by the recent experimental findings for V-flames interacting with cold walls (Jainski et al. 2017a, 2017b, 2018) and transient head-on quenching (Rißmann et al. 2017).

The main focus of most studies on FWI has been to investigate the flame dynamics during its interactions with the wall. In contrast, the effect of the flame on the near wall turbulent boundary layer flow has received limited attention. In reacting wall-bounded flows, the heat release due to combustion causes large temperature gradients and highly unsteady temperature fluctuations lead to variations in fluid viscosity and density. These variations consequently alter the turbulent boundary layer. As a result of these changes, the widely used models based on the logarithmic law-of-wall lose their validity in chemically reacting

boundary layers (Poinsot and Veynante 2005). Using DNS data (Bruneaux et al. 1996) have provided some information on the changes in the behaviour of turbulence and scalar distributions during FWI in a fully developed turbulent channel flow under constant density conditions, while (Alshaalan and Rutland 2002) interrogated DNS data by applying a quadrant splitting analysis of the Reynolds stresses in the quenching zone of a V-flame interacting with a wall. Both analysis show that there are significant differences in the turbulent boundary layer caused by the existence of the flame in the near wall region. These findings from DNS studies are supported by the experimental results (Cheng et al. 1981; Ng et al. 1982; Richard and Escudié 1999), which show that the thickness of the turbulent boundary layer increases during FWI and is explained by a higher viscosity caused by an increase in temperatures. Recent experimental findings of Jainski et al. (2018) demonstrate the changes in the Reynolds stresses within the turbulent boundary layer caused by the flame interacting with the wall which substantiates the earlier DNS findings by Bruneaux et al. (1996) and Alshaalan and Rutland (2002).

All of the aforementioned studies on turbulent boundary layers involving FWI have focused on the behaviour of turbulent boundary layer during FWI in a specific flow configuration and limited attempts have been made to investigate and compare the behaviour of turbulence across different flow configurations. Furthermore, no information exists to date in the literature regarding the influence on Reynolds stresses, wall shear stresses and the associated statistics for FWI with the variation of wall boundary conditions. Fundamental understanding of these statistics is important from the point of view of modelling FWI in engineering applications using Reynolds Averaged Navier–Stokes (RANS) or Large Eddy Simulation (LES) frameworks. In this spirit, we perform DNS of premixed flames interacting with inert walls within turbulent boundary layers under different thermal wall boundary conditions for two different flow configurations under unity Lewis number and low Mach number conditions. The first configuration consists of a V-flame interacting with inert isothermal and adiabatic walls in a turbulent channel flow configuration which leads to oblique wall interaction (OWI) of the flame. The second configuration consists of a statistically planar flame propagating into a fully turbulent boundary layer and interacting with an inert isothermal as well as an adiabatic wall, which leads to head-on interaction (HOI) of the flame. The main objectives of the present work are:

- To investigate the influence of flow configuration on the flame orientations and mean velocities during FWI within turbulent boundary layers under different thermal wall boundary conditions.
- To investigate the behaviour of wall shear stresses, wall friction velocities, Reynolds stresses and turbulence dissipation in different flow configurations under different thermal wall boundary conditions.

The rest of the paper is organised as follows: in the next section we explain the description of the flow configurations and details of the DNS data, which is followed by the discussion of the results obtained from the analysis. Finally, the conclusions are drawn and are summarised in the last section.

2 Direct Numerical Simulation Data

A well-known three-dimensional compressible DNS code SENGAs+ (Jenkins and Cant 1999) has been used to perform the simulations. The code employs high-order finite-difference schemes for spatial differentiation ranging from 10th order accuracy for internal points to 2nd order accuracy at the non-periodic boundaries, while a 3rd order explicit Runge–Kutta scheme is employed for time advancement. The governing equations of mass, momentum, energy, and species mass fractions are solved in a non-dimensional form and a single-step irreversible reaction (unit mass of *Fuel* + *s* unit mass of *Oxidiser* → (1 + *s*) unit mass of *Products*, where *s* is the stoichiometric oxidiser-fuel ratio) is used for the purpose of computational economy. This treatment for chemical reaction has been employed in several previous studies involving head-on quenching simulations of premixed turbulent flames under isotropic turbulence (Poinsot et al. 1993; Sellmann et al. 2017; Lai and Chakraborty 2016a, 2016b; Lai et al. 2017, 2018a, 2018b; Ahmed et al. 2018; Lai et al. 2017, 2018b), head-on quenching in a turbulent channel flow without density change across the flame (Bruneaux et al. 1996) and a V-flame with an isothermal wall (Alshaalan and Rutland 1998, 2002). It has also been demonstrated in previous studies that the inclusion of a detailed chemical mechanism does not alter the underlying flame dynamics, including the reaction progress variable gradient statistics, (Lai et al. 2018) or the behaviour of flame-turbulence interaction in the presence of inert isothermal walls (Ahmed et al. 2018) in spite of some differences in heat release rate behaviour in the near-wall region between simple and detailed chemistry simulations. Detailed chemistry DNS has revealed that statistics related to wall heat flux magnitude and flame quenching distance do not change between simple and detailed chemistry, and these statistics have been found to be in agreement with the corresponding values obtained from simple chemistry DNS data (Lai et al. 2018a). Furthermore, the wall heat flux and wall Peclet number obtained from simple chemistry DNS have been found to be in good agreement with experimental findings (Jarosinski 1986; Vosen et al. 1985; Huang et al. 1988). The fluid- dynamical aspects of flame-wall interaction based on simple chemistry DNS data of Alshaalan and Rutland (1998, 2002) have been found to be consistent with detailed chemistry results of Gruber et al. (2010). Furthermore, 1-D HOI simulations at different wall temperatures, ranging from 300K to 750K, with a skeletal mechanism involving 16 species and 25 reactions proposed by Smooke and Giovangigli (1991) have revealed that the variation in the dilatation rate during FWI remains almost within 3%–5% of the dilatation rate obtained from the single-step chemical reaction treatment. It is worth noting that the main focus of the current work is related to the influence of the flame on turbulence and the turbulent boundary layer during the FWI process, as the influence of chemical reaction on turbulence statistics is a consequence of dilatation rate arising from thermal expansion. Given the good agreement of dilatation rate between simple and detailed chemical mechanisms, the use of single-step chemistry does not limit the scope of the current analysis, as the current work focuses on the fluid-dynamic statistics and momentum equations do not include any explicit dependence on chemistry related terms.

The simulations presented in this work are representative of a stoichiometric methane-air mixture under atmospheric conditions, hence standard values of the Zeldovich number $\beta = T_a(T_{ad} - T_R)/T_{ad}^2$ (where T_a is the activation temperature, T_{ad} is the adiabatic flame temperature and T_R is the temperature of the reactants), Prandtl number, Pr , and ratio of specific heats, γ , (i.e., $\beta = 6.0$, $Pr = 0.7$, and $\gamma = 1.4$) are used where the Lewis numbers of all the species are taken to be unity and the species diffusion is accounted by Fick's law.

It has been shown in a DNS study of statistically planar methane-air flames with detailed chemistry and transport (Aspden et al. 2016) that the global Lewis number remains close to unity and the leading-order response of the flame speed to turbulence is primarily driven by the global Lewis number which justifies the use of unity Lewis number in this work. The heat release parameter, $\tau = (T_{ad} - T_R)/T_R$, is taken to be 2.3 for the flames considered in this work, which corresponds to preheating of reactants to a temperature of $T_R = 730$ K. This value of T_R and the resulting τ is consistent with the earlier detailed chemistry DNS of FWI in the case of a V-flame in a turbulent channel flow (Gruber et al. 2010), turbulent boundary layer flashback (Ahmed et al. 2019c, 2020; Gruber et al. 2012; Kitano et al. 2015) and single-step chemistry V-flame DNS with FWI (Alshaalan and Rutland 1998, 2002) and without FWI (Dunstan et al. 2010).

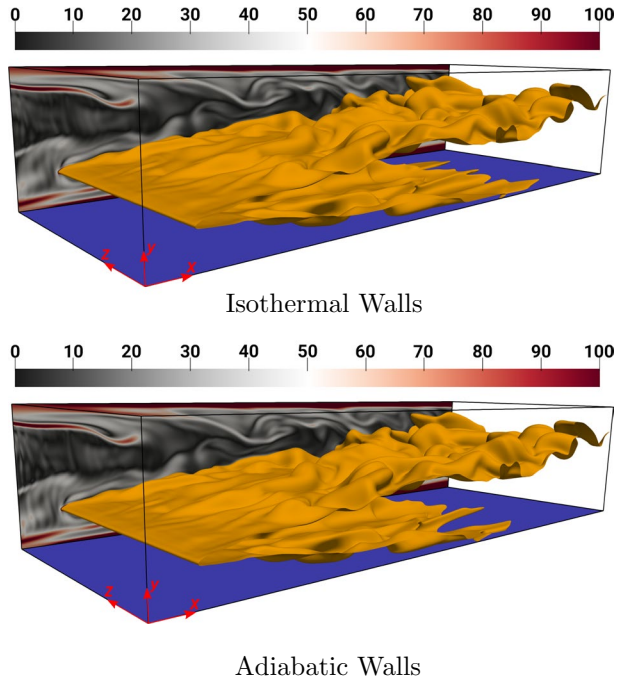
2.1 Non-reacting Turbulent Channel Flow

An auxiliary DNS of inert isothermal fully developed turbulent-plane channel flow driven by a streamwise constant pressure gradient is performed to obtain the initial turbulence conditions for both simulations and the inflow conditions for the V-flame simulation. An overall momentum balance can be used to show that the pressure gradient is directly related to the shear stress as $-\partial p/\partial x = \rho u_\tau^2/h$, where $u_\tau = \sqrt{|\tau_w|/\rho_w}$ is the friction velocity, $\tau_w = \mu_w \partial u/\partial y|_w$ is the wall shear stress, h is the channel half height, p is the pressure and μ is the dynamic viscosity of the fluid and subscript w refers to wall quantities. The bulk Reynolds number, $Re_b = \rho u_b 2h/\mu$, for this simulation is 3285, where $u_b = 1/2h \int_0^{2h} u dy$, and the wall friction based Reynolds number, $Re_\tau = \rho u_\tau h/\mu$, is 110. The grid spacing for this simulation ensures that the minimum non-dimensional distance to the wall $y^+ = \rho u_\tau y/\mu$, where y is the distance from the wall, is at most $y^+ = 0.6$ which ensures appropriate resolution of the boundary layer as recommended by Moser et al. (1999). The domain size for this channel is $10.69h \times 2h \times 4h$, which is discretised by $1920 \times 360 \times 720$ equidistant grid points. Note that all the simulations performed for this work account for compressibility effects and the Mach number, Ma , remains low i.e. $Ma = u_\tau/a = 3 \times 10^{-3}$ where a is the speed of sound.

2.2 V-flame Oblique Wall Quenching in a Turbulent Channel Flow

A flame holder is placed in the fully developed channel flow to perform the V-flame simulations, keeping the domain size and resolution the same as for the non-reacting case. The flame holder is inserted at $y^+ = 55$ from the bottom wall (i.e. $y = 0.5h$) with an approximate radius of $R_{fth} \approx 0.2\delta_{th}$, where $\delta_{th} = (T_{ad} - T_R)/\max|\nabla T|_L$ is the laminar flame thermal thickness, the subscript L represents the laminar flame quantities and $T = (\hat{T} - T_R)/(T_{ad} - T_R)$ is the non-dimensional temperature, \hat{T} being the local dimensional temperature. The centre of the flame holder is positioned at $x = 0.83h$ from the inlet of the channel. This location for the flame holder ensures that the flame interacts with the bottom wall at a reasonable distance and also that the viscous boundary layer is not influenced by the flame holder and any effects seen in the boundary layer downstream of the flame holder are due to thermal expansion arising from chemical reaction. The species, temperature and velocity distributions are imposed at the flame holder using a presumed Gaussian function following Dunstan et al. (2010). Further details on the implementation of the flame holder for this simulation are available in Ahmed et al. (2021d). In this case,

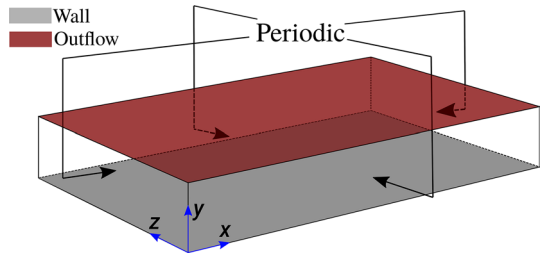
Fig. 1 V-flame with isothermal and adiabatic wall boundary conditions. The isosurface coloured in yellow represents $c = 0.5$. The instantaneous normalised vorticity magnitude Ω is shown on the $x - y$ plane. The blue surface denotes the bottom wall



the velocity fluctuations introduced at the inflow of the reacting channel are obtained by temporal sampling of the *temporally evolving turbulence* at a fixed streamwise location of the auxiliary non-reacting channel flow simulation. The time step chosen for the non-reacting simulation, while the data is being sampled, is the same as that of the reacting flow simulation.

The flow configuration for the V-flame simulations is shown in Fig. 1. Modified Navier–Stokes characteristic boundary conditions (NSCBC) due to Yoo and Im (2007) are used in the x and y directions. These boundary conditions are imposed as inflow with specified density and velocity components at $x = 0$ and partially non-reflecting outflow at $x = 10.69h$ planes; no slip conditions are imposed for velocity at the walls (i.e. $y = 0$ and $y = 2h$). The temperature boundary condition is specified using Dirichlet conditions, where the wall temperature, T_w , is the same as T_R , in the case of isothermal walls, whereas Neumann boundary conditions with zero temperature gradient, $\partial T / \partial y|_{y=0 \text{ or } y=2h} = 0$, are employed in the case of adiabatic walls. In the code the Neumann boundary condition is implemented as follows. The values for the variables (i.e. species mass fraction or temperature) at the wall are evaluated from the solution of the interior nodes adjacent to the wall during each time step and imposed as boundary conditions at the end of the respective time step. The boundaries in z direction are treated as periodic. The walls are assumed to be inert and impermeable, thus normal mass flux for all species is set to zero at the walls. The ratio of laminar flame speed to the non-reacting plane channel flow friction velocity, $S_L / u_{\tau_{NR}} = 0.7$ and δ_{th} is resolved using approximately 8 grid points. The simulations have been performed for approximately 3 flow-through times and the data has been sampled after 1 flow-through time once the initial transience have decayed. Note that under the current flow conditions 1 flow-through time is enough to obtain a statistically stationary solution for the mean turbulent kinetic energy statistics. Figure 1 shows the instantaneous

Fig. 2 Schematic of the computational domain used for the head-on interaction of the statistically planar flame across a turbulent boundary layer



flame structures represented by the progress variable $c = (Y_{F_R} - Y_F)/(Y_{F_R} - Y_{F_P}) = 0.5$ iso-surface, where Y_F is the fuel mass fraction and the subscripts R and P represent the respective values of the fuel in the unburned and fully burned gases, along with the normalised vorticity magnitude $\Omega = \sqrt{\omega_i \omega_i} \times h / \bar{u}_{\tau_{NR}}$ (where ω_i is the component of vorticity and $\bar{u}_{\tau_{NR}} = \sqrt{\bar{\tau}_{wNR}} / \bar{\rho}_{wNR}$ is the mean friction velocity of the corresponding non-reacting plane channel flow). The influence of the walls on Ω and consequently the existence of near-wall coherent flow features due to introduction of the fully developed channel flow turbulence at the inflow are clearly visible. Note that in the case of adiabatic walls the flame tends to interact with the wall further upstream when compared with the flame in the isothermal wall case which is discussed in more detail later on in the paper.

In this configuration the Reynolds averaged quantities, Favre averaged quantities, correlations involving Reynolds fluctuations (denoted by $Q' = Q - \bar{Q}$, where the overbar indicate Reynolds averaging) and Favre fluctuations (denoted by $Q'' = Q - \tilde{Q}$, where $\tilde{Q} = \overline{\rho Q / \bar{\rho}}$) have been evaluated by time averaging and subsequently using spatial averaging in the periodic (z) direction, where Q refers to a general quantity.

2.3 Planar Flame Head-on Interaction in a Turbulent Boundary Layer

The planar flame head-on interaction simulations in a turbulent boundary layer are performed by taking the solution from the fully developed turbulent channel flow up to $y/h = 1.33$ in the x and z directions. The domain size for this configuration is taken to be $10.69h \times 1.33h \times 4h$ which is discretised on $1920 \times 240 \times 720$ equidistant grid points. The boundary conditions for this case are imposed as periodic in the x and z directions and a mean streamwise pressure gradient is applied in the x direction to drive the flow, which has the same expression as for the non-reacting turbulent channel flow in sect. 2.1. The boundaries in the y direction are treated as wall at $y = 0$ where a no slip condition is imposed for velocity. The temperature boundary condition on the wall is specified using Dirichelet (i.e. $T_w = T_R$) condition in the case of isothermal wall, while a Neumann boundary condition with zero temperature gradient (i.e. $\partial T / \partial y|_{y=0} = 0$) is used in the case of adiabatic wall. An outflow boundary condition is specified at $y = 1.33h$ using the NSCBC conditions as defined by Yoo and Im (2007). The schematic of the flow configuration is presented in Fig. 2 along with the description of the boundary condition specification. It should be recognised here that this configuration is similar to the earlier work of Bruneaux et al. (1996, 1997) in a constant density turbulent channel flow. The major difference between the current simulation and the earlier simulation of Bruneaux et al. (1996, 1997) is that in the current simulation the density changes due to temperature variation and an outflow boundary

is used to avoid any unnecessary thermodynamic pressure rise as a result of density variation caused by combustion.

In these simulations an initially fully developed laminar flame from a prior 1-D flame simulation is interpolated onto the 3-D grid and specified in a manner that $c = 0.5$ is centred at $y/h \approx 0.85$. The location of the initial flame is specified such that the reactant side of the flame is facing the wall, while the product side of the flame is facing the outflow boundary in the y direction. The choice of the initial flame location and the length of the domain in the y direction is made based on the fact that the flame must remain sufficiently away from the outflow boundary at all times, while giving the flame enough time to wrinkle before interacting with the wall to obtain meaningful FWI statistics for a turbulent premixed flame. In this simulation, the ratio of laminar flame speed to the non-reacting plane channel flow friction velocity is $S_L/u_{\tau_{NR}} = 0.7$ and δ_{th} is resolved using approximately 8 grid points. In this case the boundary layer evolves slightly as the simulation progresses, but the overall simulation time remains of the order of two flow-through times, $2.0t_f$, based on the maximum streamwise mean velocity, and this simulation time is equivalent to 21.3 flame time scales defined as $t_f = \delta_{th}/S_L$. During this time the flame propagates into the reactants and moves towards the wall, consequently interacting with the wall. In the case of isothermal wall the flame quenching occurs due to wall heat loss, whereas in the case of an adiabatic wall the flame extinction occurs due to the consumption of the fuel within the domain. For the post processing of this simulation the Reynolds averaged quantities, Favre averaged quantities, correlations involving Reynolds fluctuations and Favre fluctuations have been evaluated by spatial averaging in the periodic (x and z) directions for each snapshot. The results are reported in terms of the normalised simulation time t/t_f , which is representative of the mean flame location in the y direction at a given snapshot. The instantaneous flame structures represented by the $c = 0.5$ isosurface along with the normalised vorticity magnitude Ω are shown in Fig. 3 for both wall boundary conditions. The vorticity generated in the vicinity of the wall within the turbulent boundary layer can be seen in Fig. 3. Unlike the V-flame cases there are very subtle differences in the flame structure between the two wall boundary conditions during FWI as shown in Fig. 3.

3 Results and Discussion

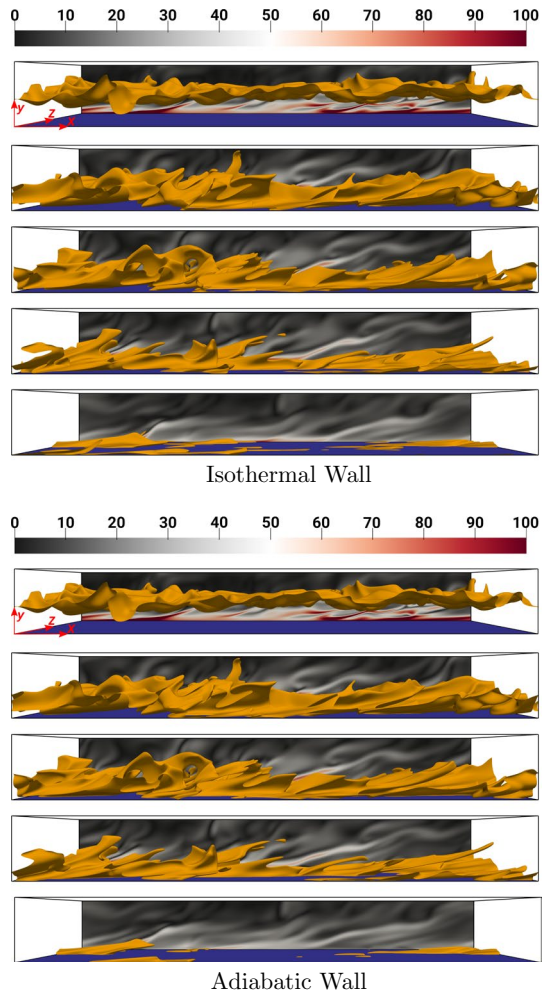
First and second moment velocity statistics of the non-reacting channel flow are first compared with reference data from literature. This is followed by a detailed discussion of the results from different reacting FWI configurations and the influence of the thermal wall boundary conditions on the turbulence related statistics.

3.1 Non-reacting Flow

The non-reacting auxiliary channel flow simulation has been compared with the results of Tsukahara et al. (2005)¹ at $Re_{\tau} = 110$ and an excellent agreement has been obtained as shown in Fig. 4, where $\bar{u}_{\tau} = \sqrt{|\bar{\tau}_w|/\bar{\rho}_w}$ is the mean wall friction velocity. These comparisons provide confidence in the set-up of the channel flow calculation which is further used for the reacting flow simulations. Figure 5 shows the evolution of the mean velocity at

¹ Database available online at: <https://www.rs.tus.ac.jp/t2lab/db/>

Fig. 3 Head-on quenching with isothermal wall boundary conditions at different time instants. From top to bottom $t/t_f = 4.20$, $t/t_f = 10.50$, $t/t_f = 11.55$, $t/t_f = 12.60$, $t/t_f = 14.70$. The isosurface coloured in yellow represents $c = 0.5$. The instantaneous normalised vorticity magnitude Ω is shown on the $x - y$ plane. The blue surface denotes the wall



two different times in the non-reacting turbulent boundary layer. Note that the non-reacting turbulent boundary layer simulation has been performed for $2.0t_F$ which is the total time taken by the flame to fully interact with the wall and consequently consume the reactants or quench depending on the wall thermal boundary condition in the case of turbulent boundary layer HOI. It can be seen in Fig. 5 that the mean velocity profiles are not significantly altered by the growth of the boundary layer at different times when compared with the non-reacting periodic channel flow. It should be noted here that the Re_τ for the current channel may be low but it has been shown in Ghai et al. (2022) that the behaviour of enstrophy, which has a close relationship with the behaviour of the dissipation rate of turbulent kinetic energy (Tennekes and Lumley 1972), normalised by wall units is not significantly affected by this and broadly remains comparable to the high Re_τ experimental results of Gorski et al. (1994).

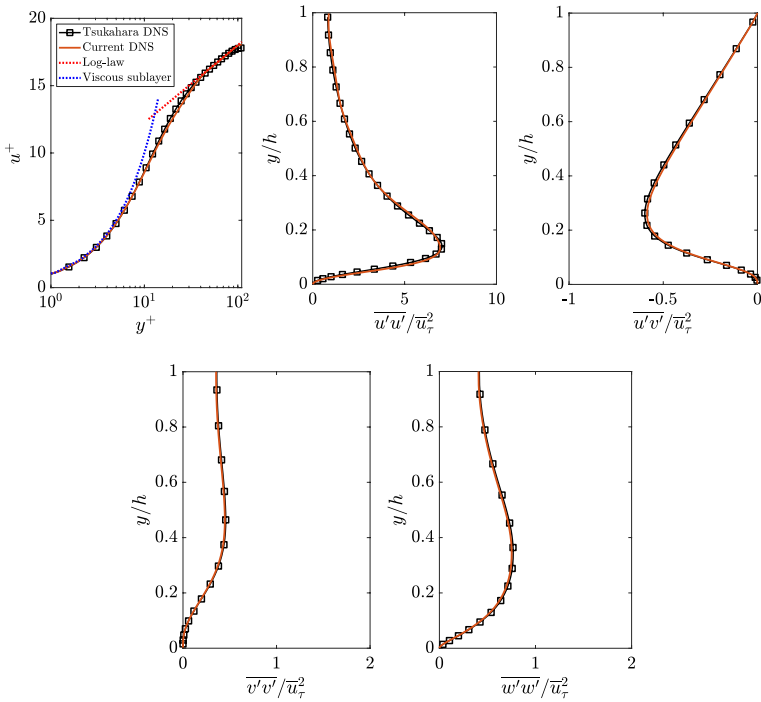
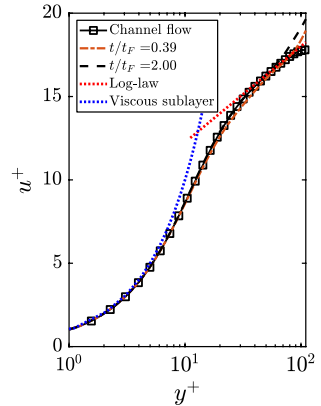


Fig. 4 Mean velocity and normalised Reynolds stresses in the auxiliary non-reacting channel flow simulation compared with the earlier DNS of Tsukahara et al. (2005) for a turbulent channel flow at $Re_\tau = 110$. Viscous sublayer means $u^+ = y^+$ and Log-law in this case is $u^+ = 2.5 \ln(y^+) + 6.5$

Fig. 5 Mean velocity in the non-reacting turbulent boundary layer flow simulation at different times compared with the non-reacting turbulent periodic channel flow at $Re_\tau = 110$. Viscous sublayer means $u^+ = y^+$ and Log-law in this case is $u^+ = 2.5 \ln(y^+) + 6.5$



3.2 Reacting Flow Behaviour

In this section, first the instantaneous flow and flame behaviour are discussed for the different flow configurations with isothermal and adiabatic wall boundary conditions. This is followed by the mean statistics for velocity and Reynolds stresses for the two flow configurations investigated.

Fig. 6 Instantaneous behaviour of the non-dimensional reaction rate of the progress variable, $\dot{\omega}_c \times \delta_{th}/(\rho_R S_L)$ along with the $c = 0.1, 0.5$ and 0.9 isolines (black lines) in the V-frame OWI configuration

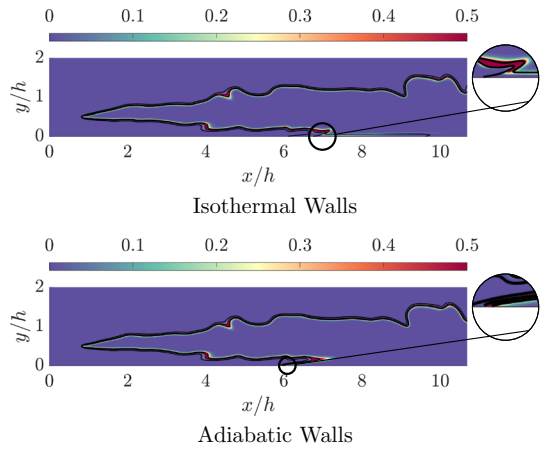


Fig. 7 Instantaneous behaviour of the non-dimensional temperature, T along with the $c = 0.1, 0.5$ and 0.9 isolines (black lines) in the V-frame OWI configuration

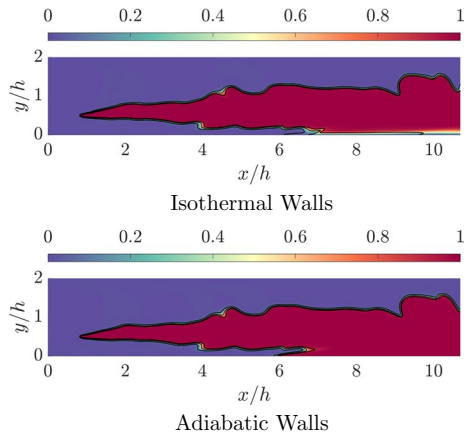
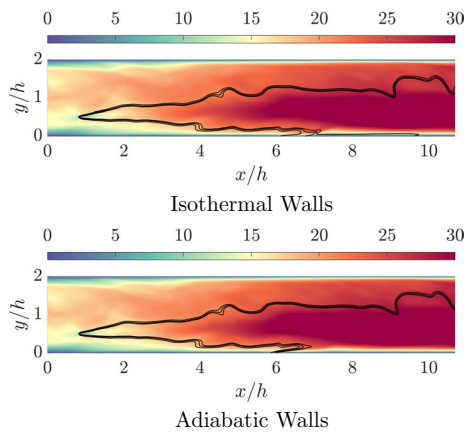


Fig. 8 Instantaneous behaviour of the non-dimensional stream-wise velocity, u/\bar{u}_{rnr} along with the $c = 0.1, 0.5$ and 0.9 isolines (black lines) in the V-frame OWI configuration



3.2.1 Instantaneous Behaviour

The instantaneous flow and flame behaviours on the $x - y$ mid-plane of the computational domain for the V-flame OWI are shown in Figs. 6, 7, 8 at the same time instants for isothermal and adiabatic wall boundary conditions, where it can be seen that the instantaneous non-dimensional temperature and the reaction rate behave differently for the two thermal wall boundary conditions. In the case of isothermal wall boundary condition the reaction rate of the progress variable diminishes as the flame approaches the bottom wall, at $y/h = 0$, due to the heat loss at the wall, whereas the reaction proceeds completely up to the wall surface in the case of adiabatic wall boundary condition. In the isothermal conditions, this leads to the development of a thermal boundary layer downstream of the flame-wall interaction region on the bottom wall and can be seen in Fig. 7. A clear decoupling between the instantaneous progress variable and the non-dimensional temperature fields near the bottom wall can be noticed for the isothermal wall conditions and is a consequence of the molecular diffusion effects of the reacting species at the bottom wall. Under these circumstances, the boundary conditions for species mass fraction and temperature are different at the isothermal wall. The species mass fraction follows a Neumann boundary condition, whereas a Dirichlet boundary condition is specified for temperature. As a result of flame quenching, the unburned reactants diffuse away from the near-wall region and their mass fraction decreases at the wall, which leads to an increase in the value for the reaction progress variable. The decoupling between the progress variable and temperature in the case of isothermal walls is consistent with several previous DNS (Bruneaux et al. 1996; Alshaaan and Rutland 1998; Gruber et al. 2010; Lai et al. 2018a; Ahmed et al. 2018) and recent experimental investigations (Jainski et al. 2017a, 2018). The decoupling between the instantaneous progress variable and the non-dimensional temperature fields does not exist for the adiabatic wall boundary conditions due to no heat loss at the wall and consequently the flame tends to interact further upstream in the case of adiabatic walls as can be noticed by the isolines of the instantaneous progress variable in Figs. 6, 7, 8. Note that when the flame is away from the wall, the temperature on the product side of the flame reaches the adiabatic flame temperature as is expected for premixed flames under low Mach and unity Lewis number conditions without any heat loss effects. In this flow configuration, under both thermal wall boundary conditions, the mean flow is in the streamwise direction while the flame is oblique to the mean flow and consequently the flow acceleration due to thermal expansion predominantly occurs in the streamwise direction and can be seen in Fig. 8 for the normalised instantaneous streamwise velocity, $u/\bar{u}_{\tau_{NR}}$, in the mean flow direction far downstream of the flame holder. It should be recognised here that the flame branch above the flame holder does not interact with the top wall at $y/h = 2$ and the overall flame behaviour in this region remains similar to the conventional unconfined V-flames in the wrinkled/corrugated flamelet regime as reported in the literature (Cheng and Shepherd 1991; Domingo et al. 2005; Dunstan et al. 2012). In both flow configurations when the flame is away from the wall the values for Damköhler number remain high (i.e. $Da \gg 1$) and Karlovitz number remains small (i.e. $Ka \ll 1$). It should also be recognised here that the integral length scale in the streamwise direction based on two-point correlation becomes large as the wall is approached for low Re_{τ} boundary layers (Ahmed et al. 2021a). This indicates that when the length scale based on two-point correlation is used the Damköhler number assumes large values, whereas vanishingly small values of Karlovitz number are obtained in the vicinity of the wall.

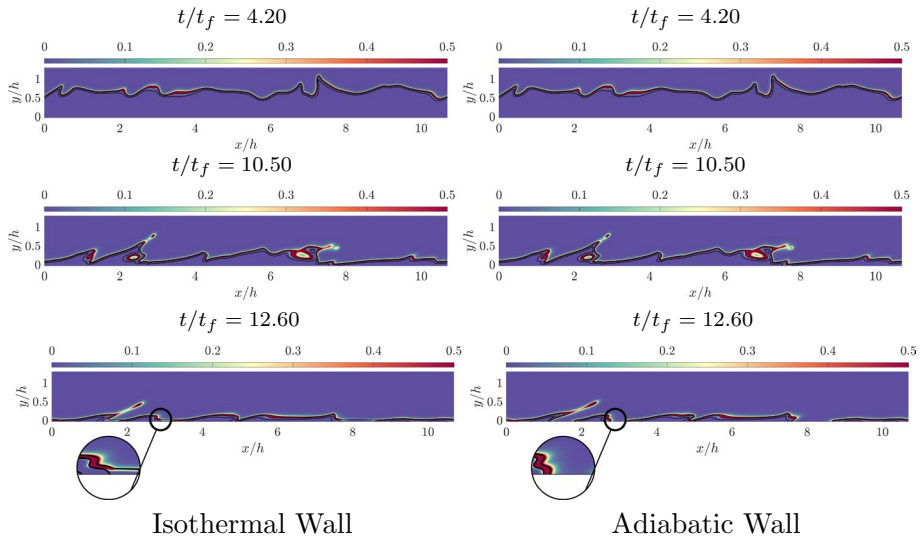


Fig. 9 Instantaneous behaviour of the non-dimensional reaction rate of the progress variable, $\dot{\omega}_c \times \delta_{th} / (\rho_R S_L)$, along with the $c = 0.1, 0.5$ and 0.9 isolines (black lines) in the turbulent boundary layer HOI configuration at different time instants

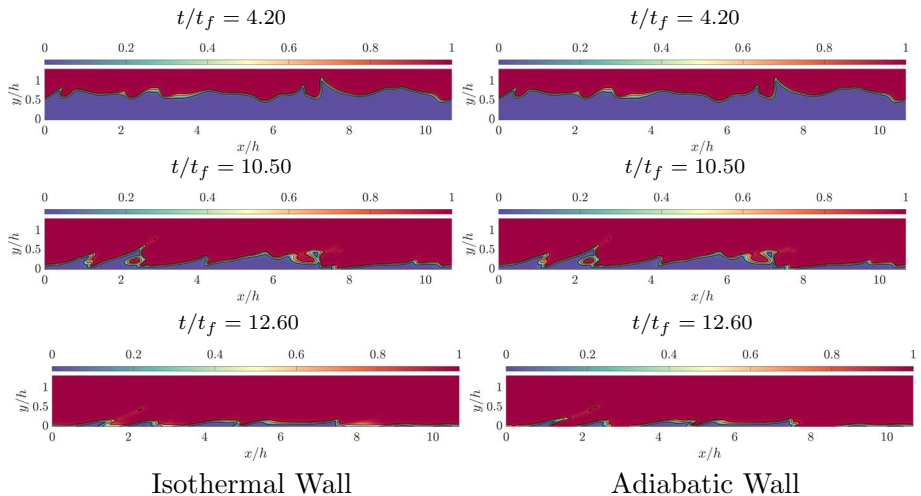


Fig. 10 Instantaneous behaviour of the non-dimensional temperature, T , along with the $c = 0.1, 0.5$ and 0.9 isolines (black lines) in the turbulent boundary layer HOI configuration at different time instants

Similar to the instantaneous flow and flame behaviour for the V-flame OWI, the turbulent boundary layer HOI at different times is shown in Figs. 9, 10, 11. In the case of both isothermal and adiabatic wall boundary conditions when the flame is away from the wall, at $t/t_f = 4.20$, the turbulence due to the fully developed boundary layer interacts with the flame and wrinkles the flame structure thus leading to a similar flame behaviour to

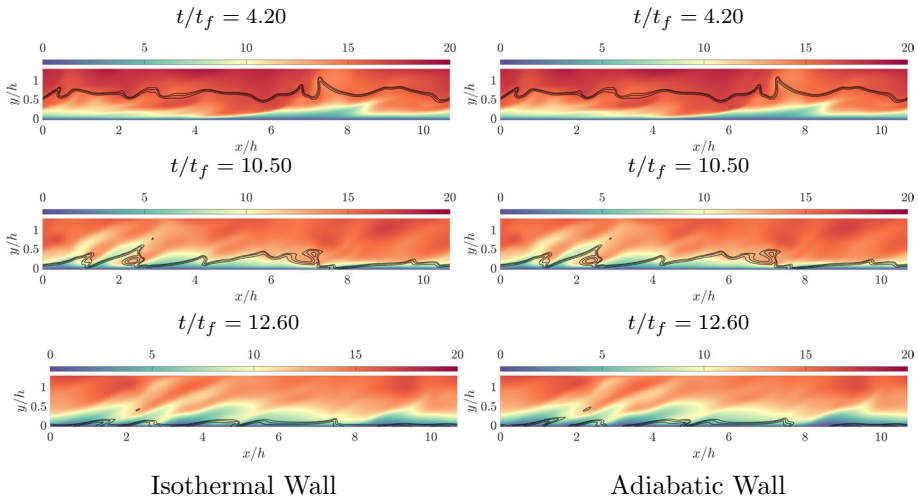


Fig. 11 Instantaneous behaviour of the non-dimensional streamwise velocity, u/\bar{u}_{NR} , along with the $c = 0.1, 0.5$ and 0.9 isolines (black lines) in the turbulent boundary layer HOI configuration at different time instants

that of a statistically planar flame in the wrinkled/corrugated flamelet regime under unity Lewis number conditions and is comparable to the flames under these conditions reported in the literature (Rutland and Cant 1994; Zhang and Rutland 1995; Cant 1999; Nishiki et al. 2002; Ahmed et al. 2019a). As the time progresses, for both thermal wall boundary conditions, the flame propagates towards the wall and consequently interacts with the wall. In the case of isothermal wall, this leads to a reduction in the reaction rate of the progress variable due to wall heat loss, which can be seen from Fig. 9. The formation of the thermal boundary layer during the FWI process is visible at $t/t_f = 12.60$ in Fig. 10 for the isothermal wall condition. By contrast, in the case of adiabatic wall condition the reaction rate remains high to the wall surface during the FWI process due to no heat loss at the wall -or formation of a thermal boundary layer- and the flame ceases to exist as a consequence of consumption of all the reactants as visible at $t/t_f = 12.60$ in Fig. 10 for the adiabatic wall condition. Similar to the V-flame OWI case a clear decoupling between the instantaneous non-dimensional temperature and the instantaneous progress variable can be noticed in Fig. 10 for the isothermal wall condition. The local wrinkling of the instantaneous flame structure can be seen in Fig. 10 for both thermal boundary conditions where it can be noticed that the flame is wrinkled due to near-wall vortical flow structures. It should be noted here that the mean flow direction in this case is the same as that in the V-flame case (i.e. in the streamwise flow direction), but the increase in velocity due to thermal expansion effects is mostly felt in the wall-normal direction and these thermal expansion effects do not significantly alter the streamwise velocity magnitude in the HOI configuration.

3.2.2 Mean Behaviour

The variation of the Favre mean progress variable in the V-flame OWI cases is presented in Fig. 12. It can be seen that the flame interacts with the bottom wall far downstream of the flame holder for both wall boundary conditions. In the case of isothermal wall boundary conditions the flame is stretched along the wall in the regions of interaction with the wall

Fig. 12 Contours of the Favre mean progress variable \tilde{c} for the V-flame OWI configuration. The dotted lines represent the locations at which the data is extracted

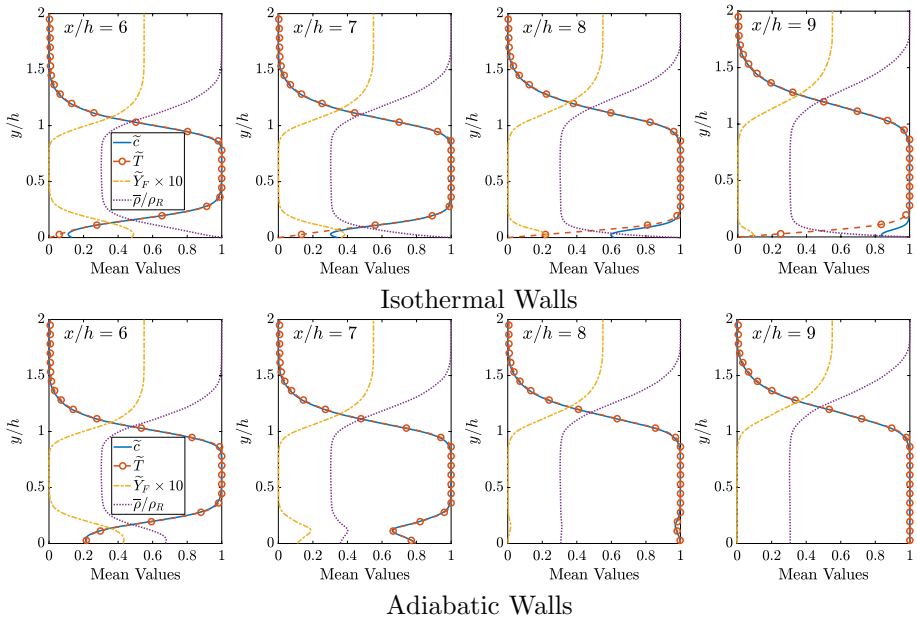
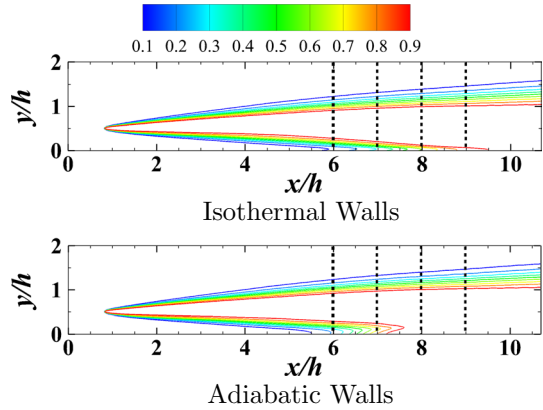


Fig. 13 Profiles for \tilde{c} , \tilde{T} , \tilde{p}/ρ_R and $\tilde{Y}_F \times 10$ in the V-flame OWI configuration at different locations downstream of the flame holder

(i.e. $5.5 < x/h < 10$). This behaviour of the flame is expected due to the diffusion of the reactants along the wall and is consistent with the earlier findings of Alshaaan and Rutland (1998, 2002) and Gruber et al. (2010) in the case of V-flame OWI DNS with isothermal wall boundary conditions. While in the case of adiabatic wall boundary conditions the flame tends to interact at upstream x/h locations (i.e. $5.5 < x/h < 8.0$), which is a consequence of the reaction rate continuing to the wall surface as there is no heat loss at the wall and the flame tends to move upstream in the low velocity near wall regions. In this work, for the V-flame OWI cases, the results are presented and comparisons are made at different

locations downstream of the flame holder where the flame interacts with the bottom wall and these locations are denoted by the dotted lines in Fig. 12. The distribution of the Reynolds averaged density, $\bar{\rho}$, normalised by the density in the unburned gases, ρ_R , Favre averaged non-dimensional temperature, \tilde{T} , fuel mass fraction, \tilde{Y}_F and progress variable, \tilde{c} for the V-flame OWI are presented in Fig. 13 at $x/h = 6, 7, 8$ and 9 locations. The difference between \tilde{c} and \tilde{T} can be seen in the case of isothermal wall boundary conditions and is expected due to the aforementioned behaviour of the respective instantaneous fields and this disparity between \tilde{c} and \tilde{T} increases with x/h . In contrast, in the case of adiabatic wall boundary conditions \tilde{c} and \tilde{T} remain coupled at all x/h locations due to the lack of wall heat loss. Note that in the V-flame OWI cases the values of \tilde{Y}_F and $\bar{\rho}$ decrease towards the centre of the channel due to the existence of the products in the wake of the flame holder. In the case of turbulent boundary layer HOI, the profiles for $\bar{\rho}$, \tilde{T} , \tilde{Y}_F and \tilde{c} are presented in Fig. 14 for both adiabatic and isothermal wall boundary conditions. In this configuration at earlier time $t/t_f = 4.20$, there is no interaction of the flame with the wall hence the profiles for \tilde{T} and \tilde{c} are identical to each other under both adiabatic and isothermal wall conditions. However, at later times (i.e. $t/t_f > 10.0$) the flame starts to interact with the wall and the differences in \tilde{c} and \tilde{T} profiles start to appear in the case of isothermal wall boundary condition. These differences in \tilde{c} and \tilde{T} become increasingly significant for isothermal wall condition, as the time progresses until all the fuel is consumed by the flame. In the case of adiabatic wall boundary condition \tilde{c} and \tilde{T} remain coupled and no differences are observed between the two. Furthermore, the flame consumes the reactants faster in the case of adiabatic wall boundary condition in the near wall region as can be noticed in Fig. 14 at $t/t_f = 16.80$ due to no heat loss at the wall. Under isothermal wall boundary condition in the case of HOI the results for \tilde{Y}_F , and \tilde{T} behave qualitatively in a similar manner to those of Bruneaux et al. (1996) for HOI in a constant density channel flow with isothermal walls. Note that at later stages of FWI (i.e. $t/t_f > 12$) under both wall boundary conditions \tilde{Y}_F is considerably lower and consequently at this stage most of the domain is filled with hot burned gases which have a lower density as demonstrated by the difference in the distribution of \tilde{Y}_F and $\bar{\rho}$ in Fig. 14.

3.2.3 Wall Heat Flux and Flame Quenching Distance Under Isothermal Wall Conditions

Wall heat flux plays an important role in determining the thermal load and cooling of combustion devices. In the case of small-sized gas turbines the heat transfer by conduction is higher than in larger engines because of the temperature gradients due to a small characteristic length (Fernandez-Pello 2002). As the characteristic length scales of the devices are reduced, the surface-to-volume ratio increases which leads to increased heat transfer effects and consequently flame quenching. Hence, the mean values of the wall heat flux into the wall must be accurately estimated for optimal design and cooling of the combustion devices. In this work the normalised wall heat flux is analysed and is defined as $\Phi_w = |q_w|/[\rho_R S_L c_{p_R} (T_{ad} - T_R)]$, where $q_w = -\lambda_w \partial \hat{T} / \partial y|_w$ is the dimensional wall heat flux, λ is the thermal conductivity of the reacting gases and c_{p_R} is the specific heat capacity of the reactants. Figure 15 shows the mean normalised wall heat flux, $\bar{\Phi}_w = |\bar{q}_w|/[\rho_R S_L c_{p_R} (T_{ad} - T_R)]$, for the two configurations under the isothermal wall conditions considered in this work. In the case of the V-flame OWI, $\bar{\Phi}_w$ is plotted along the length of the bottom wall of the channel, whereas in the case of HOI the values for $\bar{\Phi}_w$ are

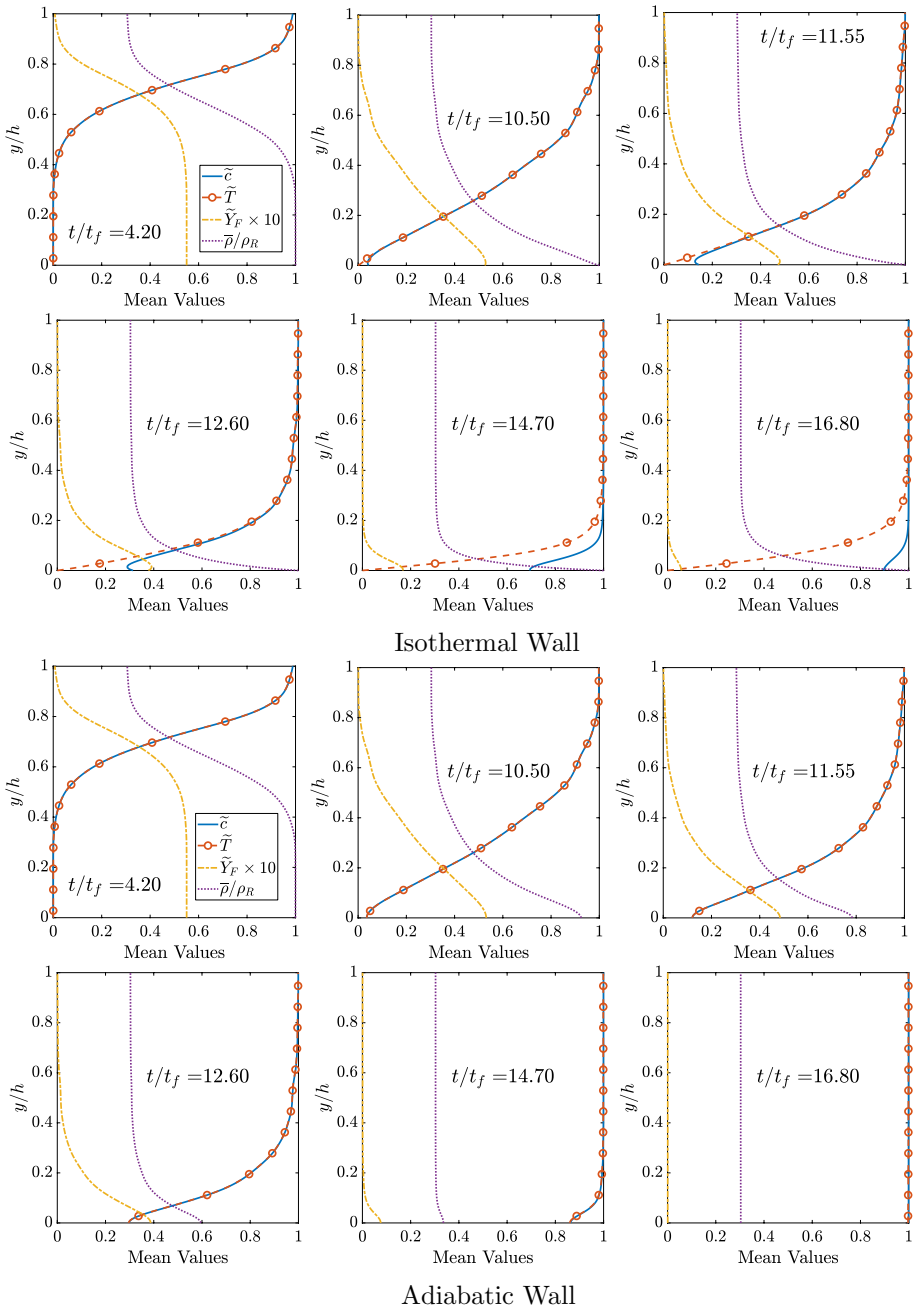


Fig. 14 Profiles for \tilde{c} , \tilde{T} , $\tilde{\rho}/\rho_R$ and $\tilde{Y}_F \times 10$ in the turbulent boundary layer HOI configuration at different time instants during FWI

plotted against time. The values of $\overline{\Phi}_w$ increase with streamwise distance in the case of V-flame OWI as the flame interacts with the wall and attains a maximum value at $x/h \approx 8$

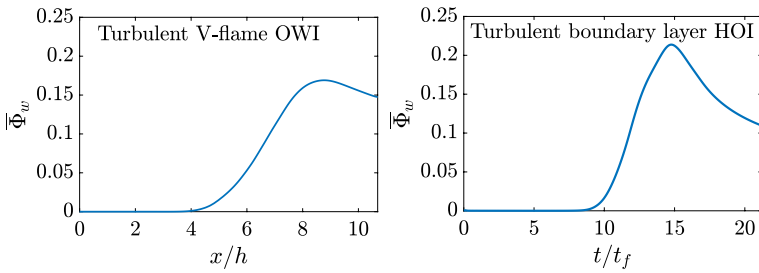


Fig. 15 The behaviour of normalised mean wall heat flux $\bar{\Phi}_w$ along the bottom wall in the streamwise direction for the V-flame OWI configuration (left) and at different time instants for the turbulent boundary layer HOI configuration (right) under isothermal wall conditions

Table 1 Values for minimum Peclet number (Pe) and maximum normalised wall heat flux (Φ_w) for different flow configurations under laminar and turbulent conditions

	Minimum Pe	Maximum Φ_w
Conventional 1-D head-on quenching	2.19	0.36
Laminar boundary layer 1-D head-on quenching	2.13	0.37
Laminar V-flame oblique wall quenching	2.41	0.31
Turbulent V-flame oblique wall quenching	1.82	0.42
Turbulent boundary layer head-on quenching	1.71	0.47

before decreasing downstream of this location due to the cooling of the hot burned products. Similarly, in the case of the turbulent boundary layer HOI configuration the values for $\bar{\Phi}_w$ increase with time as the flame interacts with the wall and attains a maximum value at $t/t_f \approx 14.7$ before decreasing due to the cooling of the burned products. These behaviours of $\bar{\Phi}_w$ are consistent with the V-flame OWI results of Alshaalani and Rutland (2002), Gruber et al. (2010) under isothermal wall boundary conditions and also with the HOI results of Bruneaux et al. (1996) under constant density and isothermal wall boundary conditions. It can be observed in Fig. 15 that the maximum $\bar{\Phi}_w$ in the case of turbulent boundary layer HOI attains a higher value when compared with the maximum value in the turbulent V-flame OWI case. This variation is a consequence of the differences in the flame and flow configuration which eventually determines the quenching distance and the orientation of the instantaneous flame structure during FWI.

In the light of $\bar{\Phi}_w$ results, it is useful to quantify the flame quenching distance δ_Q and the maximum instantaneous wall heat flux as this has major implications on the convective heat transfer to the wall which eventually determines the thermal fatigue of the combustor. In this case the Peclet number is used to determine the non-dimensional distance to the wall. The Peclet number is defined as $Pe = \delta_Q/\delta_z$, where $\delta_z = \alpha_{TR}/S_L$ is the Zeldovich flame thickens, and α_{TR} is the unburned gas thermal diffusivity. In FWI, δ_Q is taken to be the minimum wall-normal distance of the temperature isosurface at which the maximum heat release rate is obtained for an unstrained laminar flame, which for the present thermochemistry corresponds to the $T = 0.75$ isosurface. Table 1 shows the minimum instantaneous Pe and maximum instantaneous Φ_w for the two cases investigated and comparisons are made with the conventional 1-D laminar HOI under isothermal wall boundary conditions,

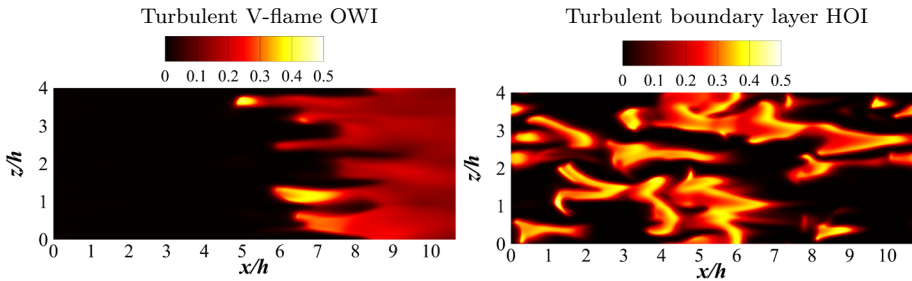


Fig. 16 The behaviour of instantaneous normalised wall heat flux, Φ_w , along the bottom wall for the V-flame OWI configuration (left) and for the turbulent boundary layer HOI configuration (right) at the time when maximum Φ_w occurs for isothermal wall conditions

where no mean flow exists, 1-D laminar boundary layer HOI under isothermal wall conditions and a V-flame OWI in a laminar channel flow with isothermal walls. Note that in all the laminar calculations the wall temperature is the same as the reactant temperature. The laminar boundary layer flow calculations have been performed by using a solution from a non-reacting laminar channel flow simulation which has the same centreline mean streamwise velocity as that of the turbulent channel flow at $Re_\tau = 110$. It can be seen in table 1 that the minimum Pe and the maximum Φ_w are comparable for the laminar HOI calculations despite the variations in the mean flow conditions, whereas the V-flame OWI under laminar conditions shows a higher value for the minimum Pe and lower value for the maximum Φ_w . These differences in the OWI and HOI cases under laminar conditions are a consequence of the flame orientation and flow shear experienced by the flame in the near wall region. Under turbulent conditions, the flames in V-flame OWI and boundary layer HOI tend to go closer to the wall resulting in lower values for minimum Pe and higher values for maximum Φ_w . This difference between the laminar and turbulent cases exists due to the interaction of flame surface with near-wall vortical flow structures, which allow for flame propagation much closer to the wall before quenching. This can be confirmed by investigating the instantaneous behaviour of Φ_w at the time instant when the maximum value of Φ_w is observed during the simulations for the V-flame OWI and HOI cases as shown in Fig. 16. In the case of HOI much higher values of Φ_w are observed when compared with the V-flame OWI case as the flame can propagate closer to the wall in the HOI case and may lead to higher thermal load on the combustor walls.

The probability density function (PDF) of Φ_w for the V-flame OWI case with isothermal walls is shown in Fig. 17 for different locations where FWI tends to occur (i.e. $x/h = 6, 7, 8$ and 9 locations) and it can be seen that the PDF for Φ_w changes shape with the streamwise distance due to the variations in the thermal boundary layer. At $x/h = 6$ and $x/h = 7$ the flame has a low probability of interacting with the wall and consequently Φ_w has the highest probability at low values. Further downstream at $x/h = 8$ and $x/h = 9$, the probability of FWI increases which leads to a higher probability of high values for Φ_w as shown in Fig. 17. The values for Φ_w at the respective x/h locations along with the maximum value of Φ_w during the simulation are also shown in Fig. 17. Comparison with the maximum value of Φ is useful from the point of view of designing combustor walls and identifying the worst case scenario. Moreover, the variation of the maximum value of instantaneous Φ_w at a given time for the head-on interaction case or at a given location in the oblique flame-interaction case is sensitive to the realisation of turbulence. Thus, a

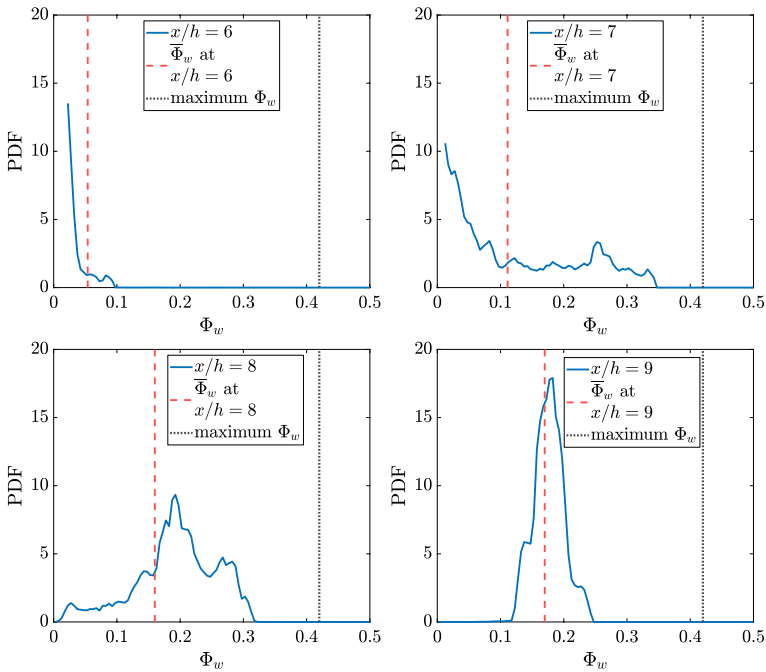


Fig. 17 Probability density function (PDF) of wall heat flux (blue line), Φ_w at different locations downstream of the flame holder in the V-flame OWI case with isothermal walls. The mean and max values of Φ_w , are shown with red and black lines respectively

different realisation of the initial condition or inlet turbulence would yield different variation of the instantaneous maximum value of Φ_w with time or distance, and thus it is difficult to interpret any trends from this information.

Figure 17 shows that the maximum value of Φ_w is well separated from the most probable value of Φ_w at all the sampling locations. This is due to the fact that the maximum value of Φ_w can occur at any location during FWI and is a consequence of the local coherent flow structure formed in the near wall region as shown in Fig. 16. Figure 18 shows the PDF of Φ_w at different time instants in the turbulent boundary layer HOI case with an isothermal wall and it can be seen that similar trends to that of the V-flame OWI case are observed. At earlier times (i.e. $t/t_f = 11.55$ and $t/t_f = 12.60$) the flame is partially interacting with the wall and consequently the highest probability is for low values of Φ_w , as shown in Fig. 18. As the probability of FWI increases with time (i.e. $t/t_f = 14.70$ and $t/t_f = 16.80$) in the HOI case, the probability for higher values of Φ_w increases. Figure 18 also shows $\overline{\Phi_w}$ at the respective time instants along with the maximum Φ_w during the turbulent boundary layer HOI simulation and similar to the V-flame OWI case, the maximum value of Φ_w tends to have a low probability and is a result of low velocity regions caused by the near-wall flow structures. This implies that $\overline{\Phi_w}$ and the PDF of Φ_w may not reflect the actual thermal load experienced by the combustor walls and the maximum values for Φ_w may need to be accounted for during the design process.

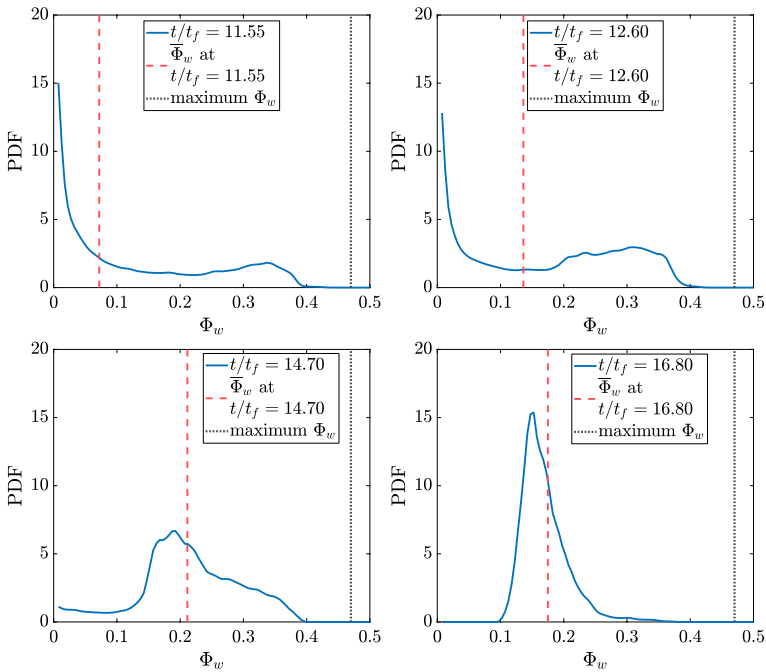


Fig. 18 Probability density function (PDF) of wall heat flux (blue line), Φ_w at different time instants for the turbulent boundary layer HOI case with isothermal wall. The mean and max values of Φ_w are shown with red and black lines respectively

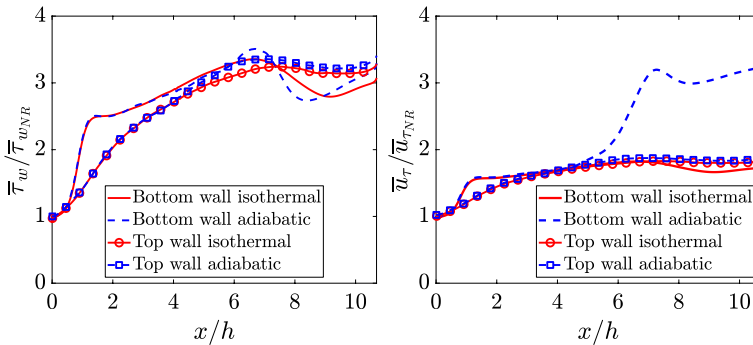


Fig. 19 Profiles for $\bar{\tau}_w$ and \bar{u}_τ along the top and bottom walls in the streamwise direction in the V-frame OWI configuration

3.3 Reacting Flow Velocity Statistics

3.3.1 Mean Velocity, Wall Shear Stress and Friction Velocity

Understanding the behaviour of mean wall shear stress, $\bar{\tau}_w$, and the mean wall friction velocity, \bar{u}_τ , during FWI is important from the point of view of understanding the turbulent

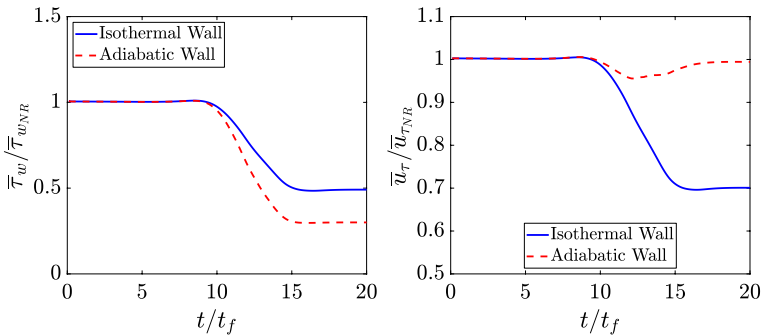
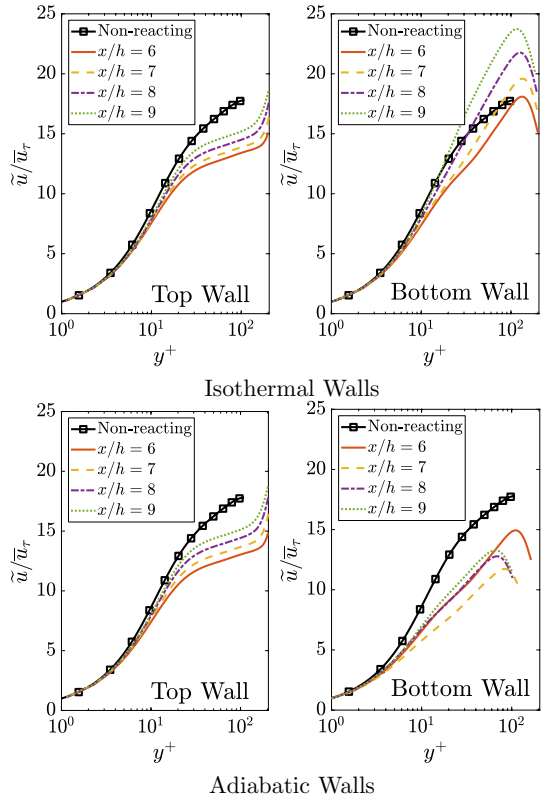


Fig. 20 Time evolution of $\bar{\tau}_w$ and \bar{u}_τ at the wall in the turbulent boundary layer HOI configuration

flow behaviour in the near wall region. In the case of V-flame OWI, the behaviours of $\bar{\tau}_w$ and \bar{u}_τ are presented in Fig. 19. Note that the values for $\bar{\tau}_w$ and \bar{u}_τ are normalised by the corresponding non-reacting values (where $\bar{\tau}_{wNR}$ is the corresponding non-reacting mean wall shear stress), so the influence of FWI and flow configuration on these quantities can be identified. Figure 19 shows that $\bar{\tau}_w$ increases on the top wall with the streamwise distance up to $x/h \approx 6$ before levelling off under both isothermal and adiabatic wall boundary conditions. This increase in $\bar{\tau}_w$ arises due to the flow acceleration in the streamwise direction caused by the thermal expansion effects of the flame and happens due to the proximity of the flame to the top wall where FWI does not take place. Overall, $\bar{\tau}_w$ behaves in a similar manner on the top wall for both adiabatic and isothermal wall conditions. On the bottom wall, under both adiabatic and isothermal wall conditions, an increase in $\bar{\tau}_w$ is seen at $x/h \approx 1$ due to the proximity of the flame holder to the bottom wall, which leads to flow acceleration further upstream when compared with the top wall. This acceleration in the streamwise velocity is a result of the thermal expansion effects of the flame and happens due to the proximity of the flame to the wall even in the absence of FWI. Further downstream, in the case of both thermal wall conditions, the values of $\bar{\tau}_w$ increase before decreasing in the region of FWI (between $x/h \approx 5.5$ and $x/h \approx 10$) and eventually tend to recover downstream of the FWI region. This decrease in $\bar{\tau}_w$ in the FWI region occurs because of an increase in the velocity in the flame normal direction, where the flame is oblique to the wall and results in the redistribution of momentum from the streamwise flow direction to the tangential direction thus reducing the streamwise component of velocity; which is discussed later on in the paper. The streamwise velocity component tends to increase further downstream resulting in steeper wall normal gradients in the near wall region which tend to enhance $\bar{\tau}_w$. Overall, the behaviour of $\bar{\tau}_w$ under both thermal wall boundary conditions is similar on the bottom wall, but a slightly higher magnitude of $\bar{\tau}_w$ variation is observed in the case of adiabatic wall conditions within the region of FWI due to a higher flow acceleration and momentum transfer from streamwise to the tangential flow direction caused by the reaction until the wall surface. It should be recognised here that despite the local reduction of $\bar{\tau}_w$ in the FWI region the value of $\bar{\tau}_w$ remains approximately three times higher than that of the corresponding non-reacting channel flow as the overall effects of thermal expansion are in the streamwise flow direction resulting in an overall higher velocity gradient at the wall. The behaviour of \bar{u}_τ follows the same trends as those of $\bar{\tau}_w$ under isothermal wall conditions, and \bar{u}_τ increases approximately by a factor of 1.7 when compared with the non-reacting channel flow, as shown in Fig. 19. Note that a

Fig. 21 Variation of \tilde{u}/\bar{u}_τ along the wall normal non-dimensional distance y^+ in the V-flame configuration at different locations downstream of the flame holder for top and bottom wall regions for top and bottom wall regions



significant increase in $\bar{\tau}_w$ can be seen in Fig. 19 on the bottom wall in the case of V-flame OWI under adiabatic wall conditions. This increase in $\bar{\tau}_w$ is a consequence of low density on the wall surface as a result of reaction occurring on the wall surface which does not happen under isothermal wall conditions due flame quenching as a result of heat loss to the wall.

The variation in the behaviour of $\bar{\tau}_w$ and \bar{u}_τ for the turbulent boundary layer HOI is shown in Fig. 20 for both thermal wall conditions. It can be seen that $\bar{\tau}_w$, when normalised by the corresponding non-reacting values, remains of the order of unity and decreases during FWI under both thermal wall boundary conditions. This decrease in $\bar{\tau}_w$ is a consequence of the redistribution of momentum from the streamwise flow direction to the direction of mean flame propagation, which is also the wall normal direction in this case. In the HOI cases, the values of \bar{u}_τ vary significantly with the change in the thermal wall boundary condition, as shown in Fig. 20. In the case of isothermal wall, the mean wall friction velocity \bar{u}_τ when normalised by the corresponding non-reacting values, decreases during FWI. However, in the case of adiabatic wall $\bar{u}_\tau/\bar{u}_{\tau NR}$ remains of the order of unity at all times. This is due to the fact that the density decreases at the wall due to the reaction up to the wall surface under adiabatic wall boundary conditions. The main difference to note between the V-flame OWI and boundary layer HOI configurations is the fact that the values of $\bar{\tau}_w$ and \bar{u}_τ do not increase above the corresponding non-reacting flow values in the turbulent boundary layer HOI, whereas a significant rise in $\bar{\tau}_w$ and \bar{u}_τ is seen in the V-flame

OWI cases due to flow confinement effects. Furthermore, the direction of the flow acceleration due to thermal expansion effect is in the streamwise direction for the V-flame OWI, whereas it happens in the wall normal direction for the case of turbulent boundary layer HOI. It should be recognised here that in case of all the simulations, different wall boundary condition as well as flame orientation with the wall, the value of τ_w decreases during FWI and the effect of variation in viscosity because of combustion on τ_w remains smaller than that of the variation in velocity gradient magnitude.

In the following analysis of the data for mean velocity and turbulence statistics in the V-flame OWI cases the domain has been divided into two parts at the centre line of the channel and is referred to as top (y/h between 1 and 2) and bottom wall regions (y/h between 0 and 1). Figure 21 shows the variation of the Favre mean non-dimensional velocity profiles for top and bottom wall regions at different locations downstream of the flame holder for isothermal and adiabatic wall boundary conditions. As shown in Fig. 19, the local value of \bar{u}_τ changes with the distance downstream of the flame holder due to flow acceleration in the streamwise direction caused by thermal expansion effects, hence the local values of \bar{u}_τ are used to evaluate \tilde{u}/\bar{u}_τ and y^+ for both top and bottom walls. The standard trend of $\tilde{u}/\bar{u}_\tau = y^+$ is obeyed in the viscous sublayer region at both walls up to $y^+ \approx 8$ under both thermal wall boundary conditions due to the use of the local values of \bar{u}_τ at each x/h location. Note that the behaviour of \tilde{u}/\bar{u}_τ is almost identical in the top wall region for the two thermal wall boundary condition as FWI does not occur on the top wall but the flame exists in proximity to the wall (at $y^+ > 10$), which results in a deviation from the non-reacting profile for \tilde{u}/\bar{u}_τ in the log-layer region of the flow.

The behaviour of \tilde{u}/\bar{u}_τ between the top and bottom wall regions is different in this flow configuration, as in the case of the top wall region the flame exists in proximity to the wall (at $y^+ > 10$) but no FWI occurs, which results in a deviation from the non-reacting profile for \tilde{u}/\bar{u}_τ in the log-layer region of the flow. In the case of isothermal walls, a lower value of \tilde{u}/\bar{u}_τ is obtained at $x/h = 6$ than the non-reacting values which progressively increases with downstream distance. While in the case of adiabatic walls a lower value of \tilde{u}/\bar{u}_τ is observed for all the sampling locations when compared with the non-reacting values. FWI tends to occur in the bottom wall region for both wall boundary conditions which significantly alters the log-layer profile for \tilde{u}/\bar{u}_τ compared with the non-reacting flow and some effects of the flame holder can also be observed at $y^+ \approx 100$, which is consistent with the earlier results of Alshalan and Rutland (1998). In general, according to Fig. 21, the FWI process tends to reduce \tilde{u}/\bar{u}_τ outside the viscous sub-layer region. In reality, the streamwise velocity increases, but the increase in the friction velocity is more rapid and implies that the scaling based on local \bar{u}_τ is not sufficient to collapse the data in the log-layer region. This in turn indicates that other mechanisms such as variations in density and the changes in the local velocity caused by flame normal acceleration of the flow are important outside the viscous sub-layer region where the flame is still active. Furthermore, the variation of \tilde{u}/\bar{u}_τ with streamwise distance exists due to the changes in the flame orientation relative to the wall as well as the mean flow direction; the inclination of the isolines of \tilde{c} with the wall changes with streamwise distance as shown in Fig. 12. This results in the redistribution of the streamwise component of velocity to that of the flame normal component within the flame and is a consequence of flow acceleration due to heat release. This can be substantiated by interrogating the behaviour of mean flow streamlines in the case of the V-flame OWI cases, as shown in Fig. 22, where the mean flow streamlines are superimposed on the mean progress variable field for both thermal wall conditions. Figure 22 shows that the direction of the mean flow streamlines changes as the values of \tilde{c} increase and the direction of the mean flow streamlines tends to move towards the flame normal direction. This

Fig. 22 Variation of mean velocity streamlines superimposed on \tilde{c} field in the V-flame configuration

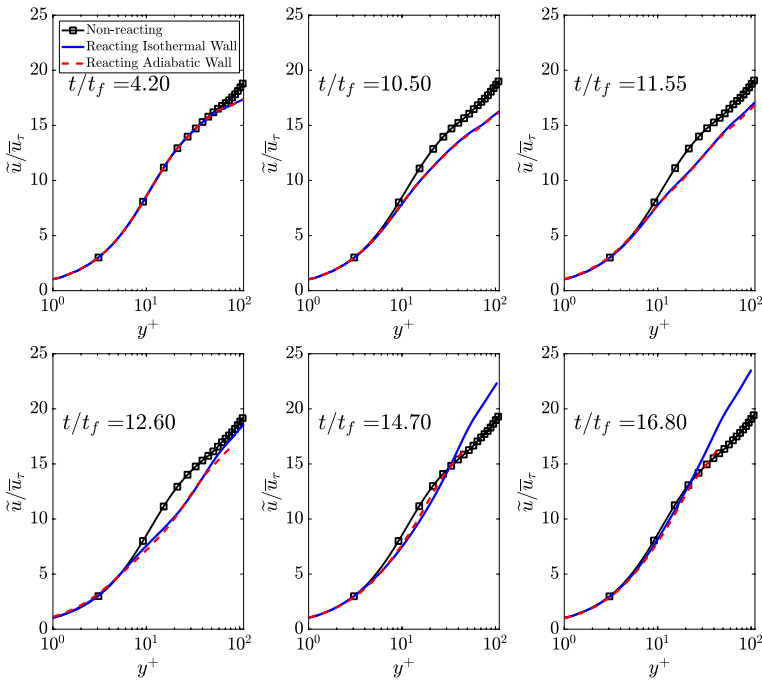
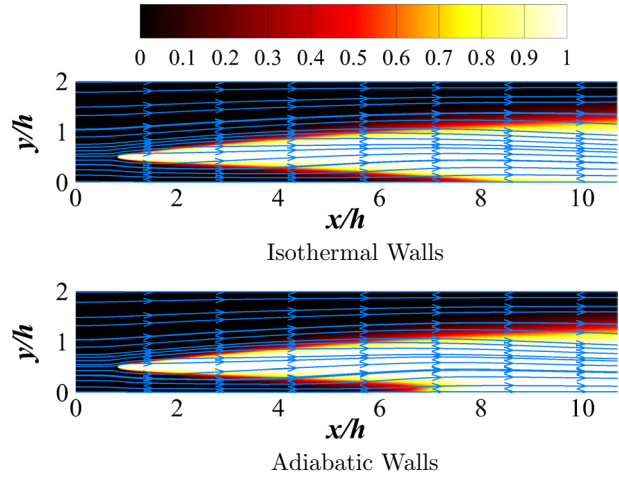


Fig. 23 Variation of \tilde{u}/\tilde{u}_τ along the wall normal non-dimensional distance y^+ at different time instants in the turbulent boundary layer HOI configuration

variation in streamlines is more pronounced in the case of adiabatic walls when compared with the isothermal wall conditions due to the density variation on the wall surface for adiabatic wall conditions.

The variation of \tilde{u}/\tilde{u}_τ with y^+ for the turbulent boundary layer HOI cases is shown in Fig. 23 for isothermal and adiabatic wall boundary conditions. A good collapse of

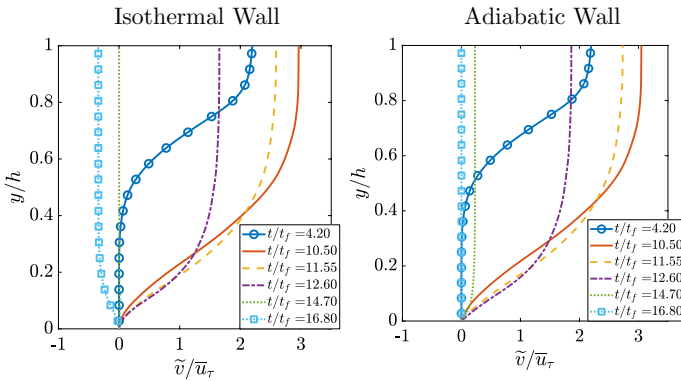


Fig. 24 Variation of \tilde{v}/\bar{u}_τ along the wall normal non-dimensional distance y/h at different time instants in the turbulent boundary layer HOI configuration

the data in the viscous sub-layer can be seen at all time instants for the reacting and non-reacting turbulent boundary layers, where the non-reacting data corresponds to exactly the same time instants as those of the reacting data. Similar to the V-flame OWI case, the local values of \bar{u}_τ have been used and consequently a disparity between the reacting and non-reacting data can be observed outside the viscous sub-layer region for all time instants presented in Fig. 23 for both thermal wall boundary conditions. At the earlier time of $t/t_f = 4.20$ the influence of the flame is only seen in the log-layer region and a drop in \tilde{u}/\bar{u}_τ can be seen when compared with the non-reacting turbulent boundary layer at the same time instant. The behaviour of \bar{u}_τ at earlier times when the flame is away from the wall (i.e. $t/t_f < 10$) or at the earlier stages of FWI (i.e. $10 < t/t_f < 11.55$) is similar for both thermal wall boundary conditions. This trend continues until almost all of the fuel is consumed and at that stage \tilde{u}/\bar{u}_τ in the reacting turbulent boundary layer with isothermal wall tends to increase and becomes larger than the non-reacting counterpart, while \tilde{u}/\bar{u}_τ in the reacting turbulent boundary layer with the adiabatic wall tends to decrease. As shown earlier, in the case of HOI with isothermal wall the values for \bar{u}_τ decrease substantially during the FWI process while \bar{u}_τ remains almost unaffected in the case of HOI with adiabatic wall, thus \bar{u}_τ is not responsible for the decrease in \tilde{u}/\bar{u}_τ in the log-layer region at earlier times. This decrease is primarily caused by the redistribution of the streamwise velocity to the flame normal component of the velocity - which in this configuration is also the wall normal component - caused by the thermal expansion effects. This redistribution of velocity occurs until the flame is quenched by the cold wall and the effects of the redistribution of velocity weaken as the time progresses. This can be substantiated by plotting the variation of \tilde{v}/\bar{u}_τ at different time instants in the turbulent boundary layer HOI cases, as shown in Fig. 24. Note that for the non-reacting flow in the same configuration, the mean wall normal component of velocity remains zero and any rise in the mean wall normal component of velocity in the reacting cases is due to the thermal expansion effects of the flame. At later time (i.e. $t/t_f > 14.70$), for the HOI case with isothermal wall, \tilde{u}/\bar{u}_τ increases in the log-layer region when compared with the non-reacting counterpart and this increase in velocity is caused by the reduction in the redistribution

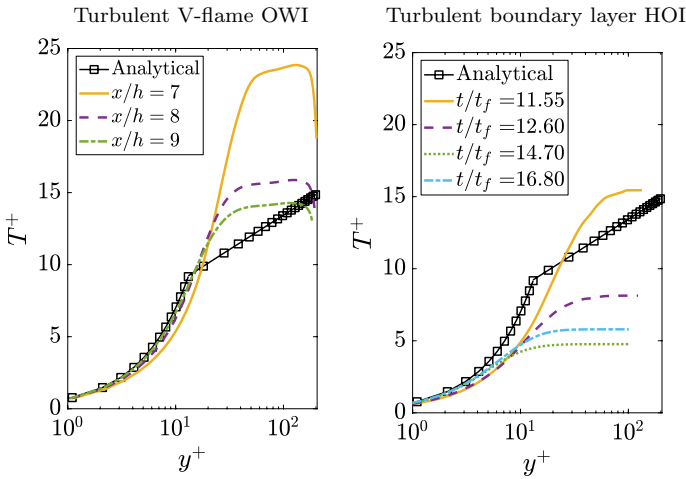


Fig. 25 Variation of T^+ along y^+ in the bottom wall region of the V-flame OWI configuration with isothermal walls at different locations downstream of the flame holder (left) and at different time instants during FWI in the turbulent boundary layer HOI configuration with isothermal wall (right)

of the mean streamwise velocity in the wall normal direction, as evident from Fig. 24 and also due to the fact that the value of \bar{u}_τ has decreased substantially by this time thus leading to a higher value for \tilde{u}/\bar{u}_τ . Contrary to this at later times (i.e. $t/t_f > 14.70$) in the HOI case with adiabatic wall, \tilde{u}/\bar{u}_τ tends to behave similar to that of the non-reacting counterpart as the value of \bar{u}_τ remains largely unaffected by the FWI process. This implies that like the V-flame OWI the scaling of the mean velocities with local \bar{u}_τ for the turbulent boundary layer HOI collapses the data with the non-reacting flow velocities in the viscous sub-layer region, but is not sufficient to collapse the data in the log-layer region. The flame introduces additional turbulent transport mechanisms that are not present in non-reacting flows without heat release, in particular the mean pressure gradient and pressure dilatation effects within the flame (Zhang and Rutland 1995; Chakraborty et al. 2011).

3.3.2 Mean Temperature in Wall units under Isothermal Wall Conditions

The non-dimensional temperature using wall units, $T^+ = (\tilde{T}/\bar{\Phi}_w) \times \bar{u}_\tau/S_L$, is presented in Fig. 25 for different locations downstream of the flame holder in the bottom wall region of the V-flame OWI with isothermal walls and at different time instants during FWI for the turbulent boundary layer HOI case with isothermal wall. The results from both cases are compared with the analytical expression for T^+ proposed by Kays and Crawford (1993) for flows without reaction in fully developed turbulence and turbulent heat flux based on the Reynolds analogy. The analytical expression reads $T^+ = (Pr_t/\kappa) \ln(y^+/y_{crit}^+) + y_{crit}^+ Pr_t$, where Pr_t is the turbulent Prandtl number, κ is the Von Karman constant and y_{crit}^+ is the thermal sublayer thickness in wall units. This expression holds for $y^+ > 30Pr_t$ (Kays and Crawford 1993) suggest: $Pr_t = 0.85$, $\kappa = 0.41$ and $y_{crit}^+ = 13.2$. In the case of the V-flame OWI case with isothermal wall, the results are presented for the bottom wall region as FWI only occurs on the bottom wall and the influence of the flame holder on the T^+ profile can be seen at $y^+ \approx 55$ in Fig. 25. It can also be noticed in Fig. 25 that T^+ profiles

are in reasonable agreement with the analytical profile in the viscous sub-layer region for both cases, beyond which a significant deviation occurs in the log-layer region for all the sampling locations and times, which is a consequence of the variations in the values of $\overline{\Phi_w}$. In the case of V-flame OWI, a higher value of T^+ is observed where $\overline{\Phi_w}$ is low (i.e. $x/h = 7$, see Fig. 15 for details on $\overline{\Phi_w}$) and decreases with increasing values of $\overline{\Phi_w}$. Figure 25 further reveals that the shape of the profile for T^+ is significantly different from the one obtained from the analytical expression, even for the locations at which the magnitude of T^+ is similar to the one obtained from the analytical expression. Similar trends for T^+ are observed in the case of turbulent boundary layer HOI with isothermal wall and do not match with the analytical profile in the log-layer region. At the earlier stages of FWI, the values for $\overline{\Phi_w}$ are low (see Fig. 15) and consequently higher values of T^+ are observed in the log-layer region and these values decrease at the later stages of FWI when $\overline{\Phi_w}$ decreases.

3.3.3 Mean Reynolds Stresses and Dissipation of Turbulent Kinetic Energy

In order to investigate the influence of FWI within turbulent boundary layers on the near-wall turbulence the variation of Favre mean Reynolds stresses, $\overline{u_i''u_j''}$, turbulent kinetic energy, $\tilde{k} = \overline{u_k''u_k''}/2$, and turbulence dissipation $\tilde{\epsilon} = \overline{\mu(\partial u_i''/\partial x_j)(\partial u_i''/\partial x_j)}/\rho$, are investigated for the two flow configurations considered in this work. The results for the aforementioned quantities are normalised by $\overline{u_{\epsilon_{NR}}}$, due to the issues mentioned in sect. 3.3.1 that the normalisation with the local value of the friction velocity leads to a good collapse of the data in the viscous sub-layer region of the flow but the collapse of the data in the log-layer region where the influence of heat release due to chemical reaction is large gets significantly affected by this scaling. This implies that the scaling with the local friction velocity may lead to an under or over estimation of the Reynolds stresses and turbulence dissipation, thus leading to erroneous conclusions. Figures 26 and 27 show the variations of $\overline{u_i''u_j''}$, \tilde{k} and $\tilde{\epsilon}$ in the top and bottom wall regions of the channel in the case of the turbulent V-flame OWI cases for both thermal wall boundary conditions. The flame does not interact with the wall in the top wall region, but is in close proximity to it, so there is a significant influence on the behaviour of the underlying turbulence of the flow and the behaviour of the turbulent boundary layer, as shown in Fig. 26. Note that in the top wall region of the V-flame OWI cases, the mean flame brush represented by $0.0 < \tilde{c} < 1.0$ exists beyond $y/h \approx 0.5$ (see Fig. 12) and a significant deviation in the behaviour of $\overline{u_i''u_j''}$ between non-reacting channel and V-flame OWI results can be observed. It can be noticed from Fig. 26 that the streamwise component of the Reynolds stress, $\overline{u''u''}$, is the dominant contributor to \tilde{k} for both thermal wall boundary conditions and the maximum values of $\overline{u''u''}$ and \tilde{k} occur much closer to the top wall when compared with the non-reacting channel flow. The magnitudes of $\overline{u''u''}$ and \tilde{k} are significantly lower at $x/h = 6$ for both thermal wall boundary conditions when compared with the non-reacting channel flow and progressively increase with the downstream distance approaching to that of the non-reacting flow at $x/h = 9$. This is a result of a decrease in the streamwise flow velocity as discussed in sect. 3.3.1 which also has a significant influence on the other Reynolds stress components, especially on $\overline{u''v''}$ and $\overline{w''w''}$ components, as shown Fig. 26. The values for $\tilde{\epsilon}$ are higher in the near wall region for the top wall ($y/h < 0.1$) due to a local flow acceleration in the streamwise flow direction resulting in steeper velocity gradients in this region as evident from $\overline{\tau_w}$ in Fig. 19. Further away from the top wall the behaviour of $\tilde{\epsilon}$ is similar to the non-reacting

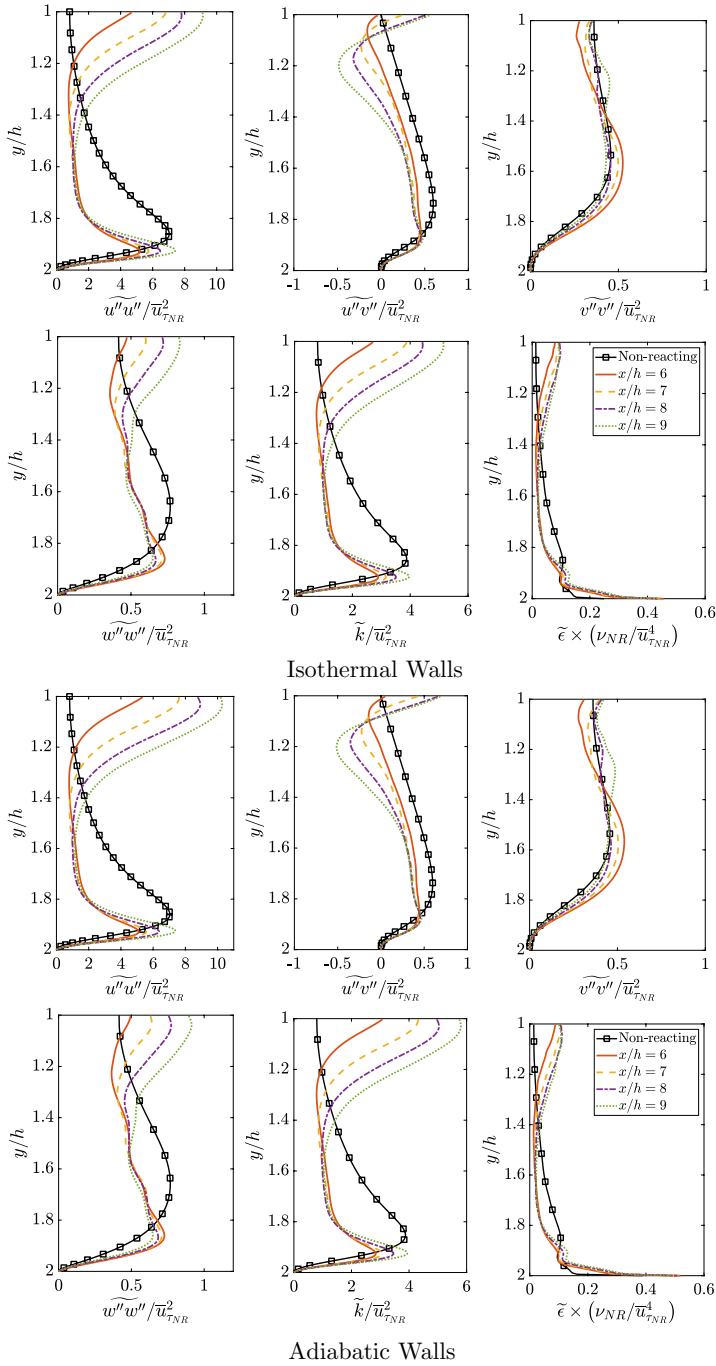


Fig. 26 Profiles for normalised Reynolds stresses, $\overline{u''_i u''_j}$, turbulent kinetic energy, \tilde{k} , and turbulence dissipation, $\tilde{\epsilon}$ in the top wall region of the V-flame OWI configuration at different x/h locations downstream of the flame holder

channel flow in an order of magnitude sense, but some differences between reacting and non-reacting profiles exist due to the presence of the flame (see Fig. 26). Overall, the behaviour of the turbulence quantities is not significantly affected by the change in the thermal wall boundary conditions for the top wall as the flame does not interact with the wall and only remains in proximity to the wall.

The behaviour of $\overline{u_i''u_j''}$, \tilde{k} and $\tilde{\epsilon}$ in the bottom wall region of the V-flame OWI for both thermal wall boundary conditions is presented in Fig. 27. The behaviour of these quantities is significantly different from the non-reacting channel flow and also from the top wall region due to the interaction of the flame with the bottom wall. Similar to the non-reacting channel flow and the top wall region of the V-flame OWI cases $\overline{u''u''}$ dominates the contribution to \tilde{k} under both thermal wall boundary conditions. A significant reduction in $\overline{u''u''}$ and \tilde{k} can be seen in the region $y/h < 0.2$ for all the streamwise sampling locations due to the redistribution of the velocity from the mean streamwise component to the flame normal component as explained in sect. 3.3.1 for both thermal wall boundary conditions. Further away from the wall, at $y/h > 0.2$, the values of $\overline{u''u''}$ and \tilde{k} increase due to shearing of the flow as a result of density variations caused by the flame. Figure 27 shows that all the major components of the Reynolds stress are significantly affected by the existence of the flame. Some subtle differences in the magnitudes of $\overline{u''u''}$ can be seen between the two wall boundary conditions, where the V-flame OWI case with adiabatic walls shows slightly larger magnitudes, while major differences in the $\overline{v''v''}$ and $\overline{w''w''}$ components of the Reynolds stress are observed at $x/h = 7$. These differences between the isothermal and adiabatic walls exist due to the reaction proceeding completely up to the wall surface in the case with adiabatic walls and the region of maximum mean heat release is located roughly at $x/h = 7$ (see Fig. 12 where $\tilde{c} = 0.7$ is located at $x/h = 7$). Note that in the V-flame OWI cases the flame holder exists at $y/h = 0.5$ from the bottom wall and effects on $\overline{u_i''u_j''}$ from the flame branch above the flame holder are present in the bottom wall region at $y/h > 0.5$ at all sampling locations. Similar to the top wall region the values for $\tilde{\epsilon}$ increase in the near wall region and are higher than the non-reacting counterpart channel flow data, as shown in Fig. 27. The flow acceleration due to heat release in the near wall region leads to higher velocity gradients which result in higher values of $\tilde{\epsilon}$ in the case of the bottom wall for the V-flame OWI cases, especially for the case with adiabatic walls. Unlike the top wall region, the values for $\tilde{\epsilon}$ remain higher than the non-reacting channel flow in the bottom wall region for all locations away from the wall. This is a consequence of higher flow velocities due to flow confinement downstream of the flame holder and higher \tilde{k} in this region.

The Reynolds stress anisotropy, $b_{ij} = \overline{u_i''u_j''}/\overline{u_k''u_k''} - (1/3\delta_{ij})$, for both top and bottom wall regions in the V-flame OWI flow is shown in Fig. 28 on the Lumley triangle where $\eta = \sqrt{(b_{ij}b_{ji})/6}$ and $\xi = \sqrt[3]{(b_{ij}b_{jk}b_{ki})/6}$ (Pope 2000). The non-reacting channel flow results are also plotted in Fig. 28 for comparison with the V-flame OWI results with adiabatic and isothermal wall boundary conditions. In the case of the non-reacting flow the Reynolds stresses are anisotropic tending towards the one and two component limit in the near wall region and become isotropic towards the centre of the channel which is consistent with the results of Kim et al. (1987) as shown by Pope (2000). Note that the values of y^+ in this case are evaluated based on the local $\overline{u_\tau}$ values to be consistent with the earlier results of $\tilde{u}/\overline{u_\tau}$ in sect. 3.3.1, which helps in the identification of the viscous sub-layer and the log-layer regions of the flow. In the top wall region, where no FWI occurs, in the V-flame OWI cases the Reynolds stresses tend to behave in a similar manner to that of the non-reacting channel

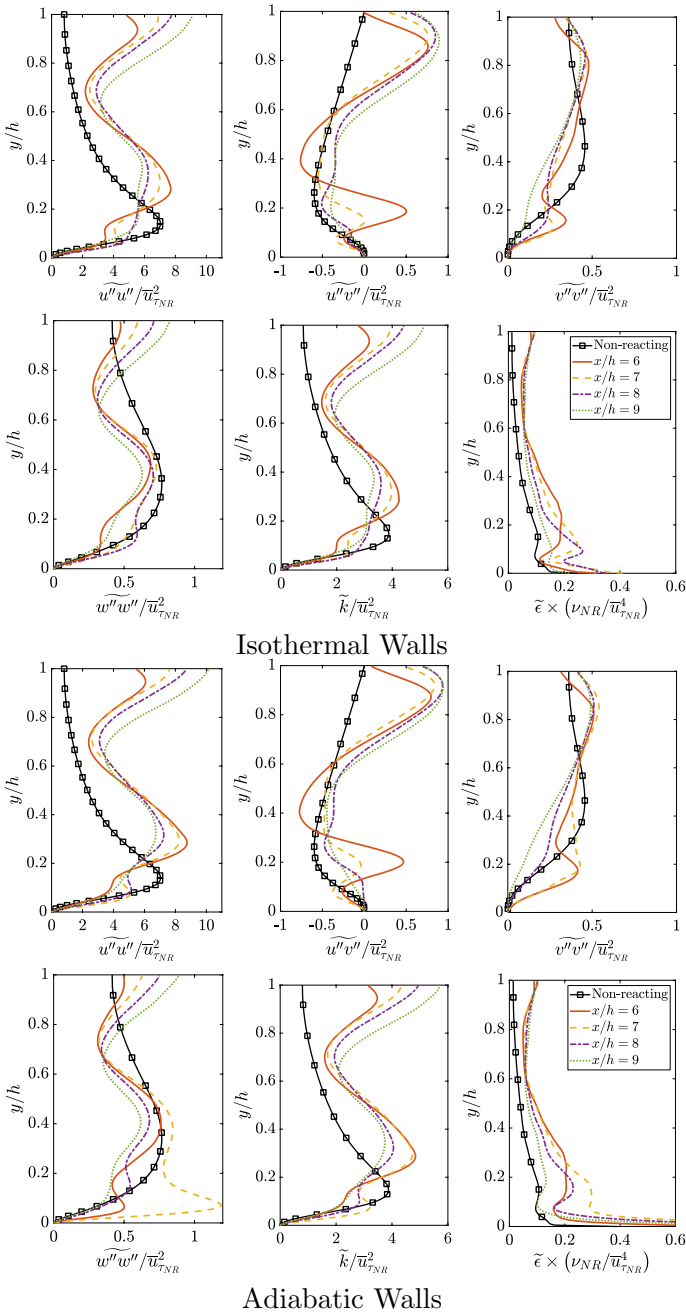


Fig. 27 Profiles for normalised Reynolds stresses, $\overline{u''u''}$, turbulent kinetic energy, \tilde{k} , and turbulence dissipation, $\tilde{\epsilon}$ in the bottom wall region of the V-flame OWI configuration at different locations downstream of the flame holder

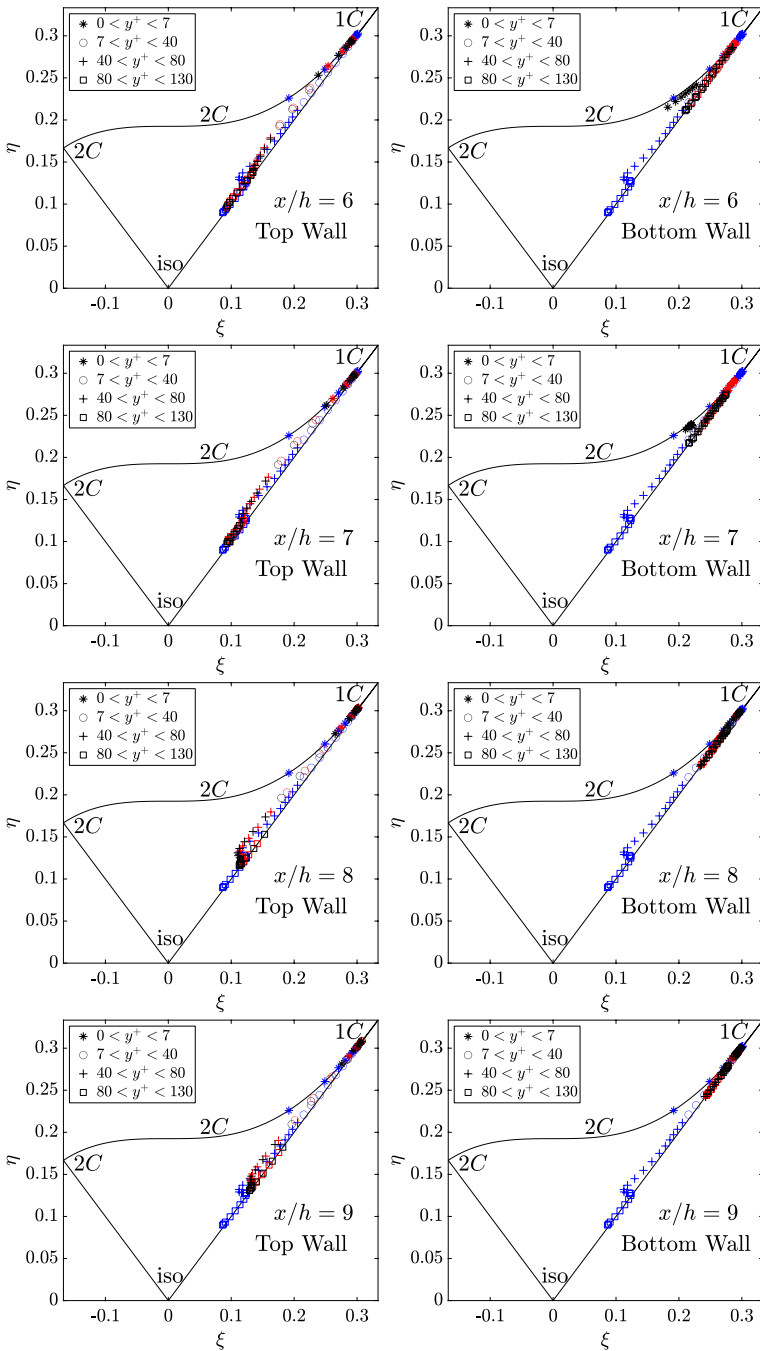


Fig. 28 Lumley triangle on the plane of the invariants η and ξ of the Reynolds stress anisotropy tensor in the top (left) and bottom (right) wall regions of the V-flame OWI configuration with isothermal (red symbols) and adiabatic (black symbols) wall conditions at different downstream locations of the flame holder compared with the non-reacting channel flow (blue symbols). 1C, 2C and iso imply 1 component limit, two component limit and isotropic state respectively

flow for $x/h = 6$, $x/h = 7$, but further downstream at $x/h = 8$ and $x/h = 9$ the Reynolds stresses in the log-layer region of the flow ($80 < y^+ < 130$) tend to deviate from the non-reacting flow data due to the existence of the top branch of the flame above the flame holder in the V-flame OWI channel flow with isothermal as well as adiabatic walls. In the bottom wall region where FWI occurs the Reynolds stresses tend towards the one component limit for all the sampling locations due to the anisotropy introduced by the existence of the flame. This phenomenon exists for low turbulence intensity flames at high Damköhler number conditions (Ahmed et al. 2019b; Brearley et al. 2019, 2020; Chakraborty 2021) and as stated earlier on in the paper the integral length scale based on the two-point correlation is large and remains of the order of $1.5h$ in the near wall region at low Re_τ conditions (Ahmed et al. 2021a) which results in a flame at high Damköhler number conditions due to low turbulence intensity and large length scales in this case. It should be noted here that subtle differences in the Reynolds stress anisotropy between the V-flame OWI with isothermal and adiabatic walls exist at $x/h = 6$ and $x/h = 7$ in the bottom wall region where more contribution to the two component limit at low y^+ values exists which is a consequence of density variation at the wall surface in the case of adiabatic wall boundary conditions.

Figure 29 shows the behaviour of $\overline{u_i''u_j''}$, \tilde{k} and $\tilde{\epsilon}$ in the case of turbulent boundary layer HOI at different times for both thermal wall boundary conditions. In these cases the data is compared with the non-reacting simulation for the same configuration at the same time instants as those for the reacting simulations. At earlier times when the flame is away from the wall the turbulence statistics are not significantly affected by the flame in the near wall region for both thermal wall boundary conditions, as shown in Fig. 29 and some influence of the effects of heat release can be seen at $y/h \approx 0.8$. As the time progresses and the flame propagates towards the wall the $\overline{u''v''}$, $\overline{v''v''}$ and $\overline{w''w''}$ components of the Reynolds stresses are significantly affected by the flame under both adiabatic as well as isothermal wall conditions (see Fig. 29). The main reason for the significant variation of $\overline{u''v''}$ and $\overline{v''v''}$ components of the Reynolds stress is the redistribution of the velocity from the streamwise component to the transverse component as discussed in sect. 3.3.1. During the FWI process the turbulence decays rapidly and all the components of $\overline{u_i''u_j''}$ reduce in magnitude which is similar to the earlier results of Bruneaux et al. (1996) in a constant density turbulent channel flow. Note that similar to the V-flame OWI cases, the $\overline{u''u''}$ component of the Reynolds stresses dominates the contribution to \tilde{k} but unlike the V-flame OWI cases both quantities decay as the flame interacts with the wall. This is due to the fact that in the case of V-flame OWI, the flow acceleration due to thermal expansion has a component parallel to the wall which produces shear and generates turbulence, whereas in the case of turbulent boundary layer HOI the thermal expansion effects are in the wall normal direction which tend to decrease turbulence. The behaviour of $\tilde{\epsilon}$ in the turbulent boundary layer HOI cases follow the same trends as that of $\overline{u_i''u_j''}$ and decay in the near wall region during FWI when compared with the non-reacting flow, as shown in Fig. 29. Note that, during the FWI process (i.e. $10.50 < t/t_f < 14.70$), the magnitude of $\overline{u_i''u_j''}$, \tilde{k} and $\tilde{\epsilon}$ is higher in the case of adiabatic wall due to the reaction occurring until the wall surface, which generates higher wall normal velocity in this case resulting in the generation of turbulence.

The behaviour of the anisotropy of the Reynolds stresses for the turbulent boundary layer HOI cases and the corresponding non-reacting flow is shown in Fig. 30 at different times during the HOI process. In this case the non-reacting flow behaviour is similar to that of the non-reacting turbulent channel flow. At earlier times when the flame is away from the wall (i.e. $t/t_f \approx 4.20$) the Reynolds stress anisotropy is affected only at high y^+

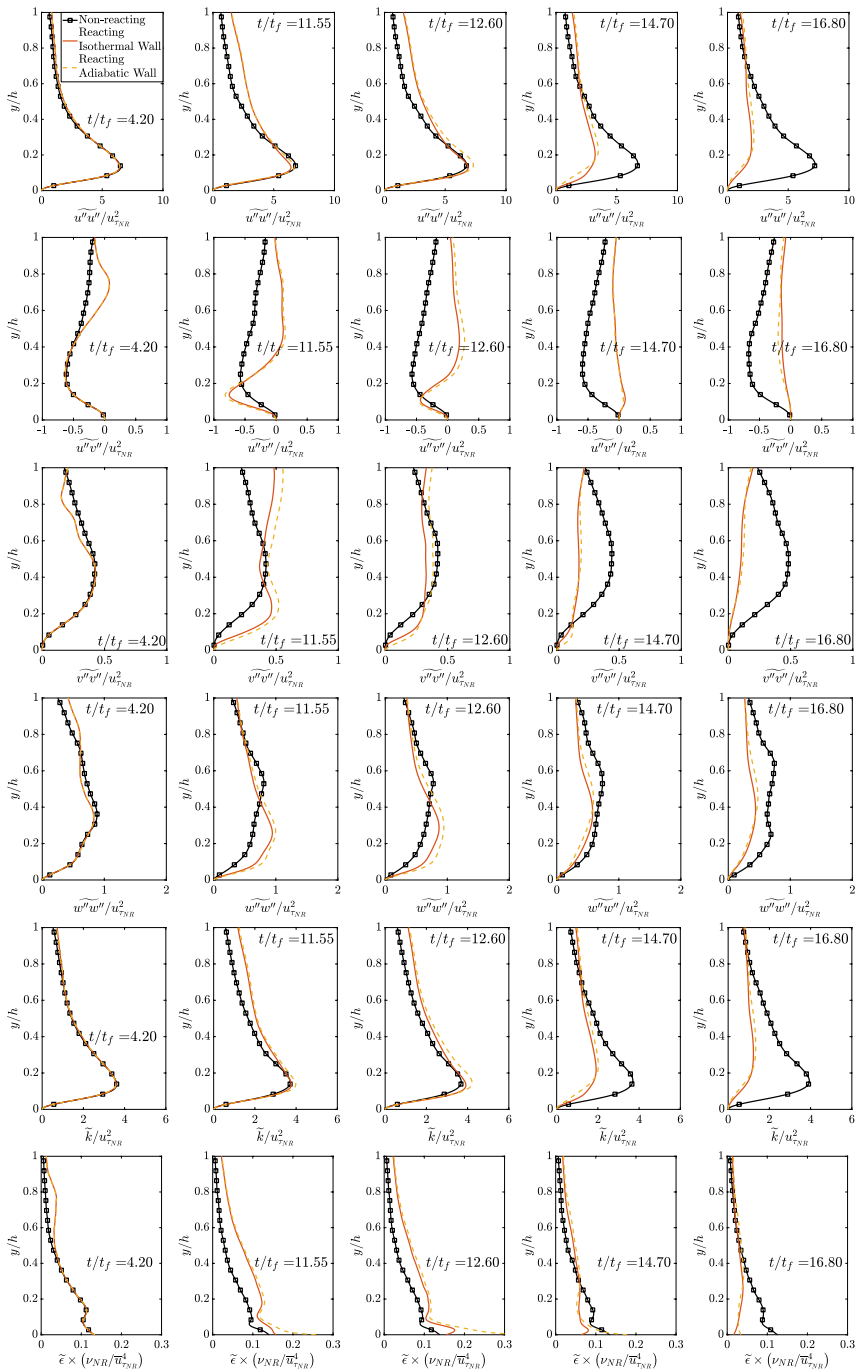


Fig. 29 Profiles for normalised Reynolds stresses, $\overline{u''u''}$, turbulent kinetic energy, \tilde{k} , and turbulence dissipation, $\tilde{\epsilon}$ at different time instants during FWI for the turbulent boundary layer HOI configuration

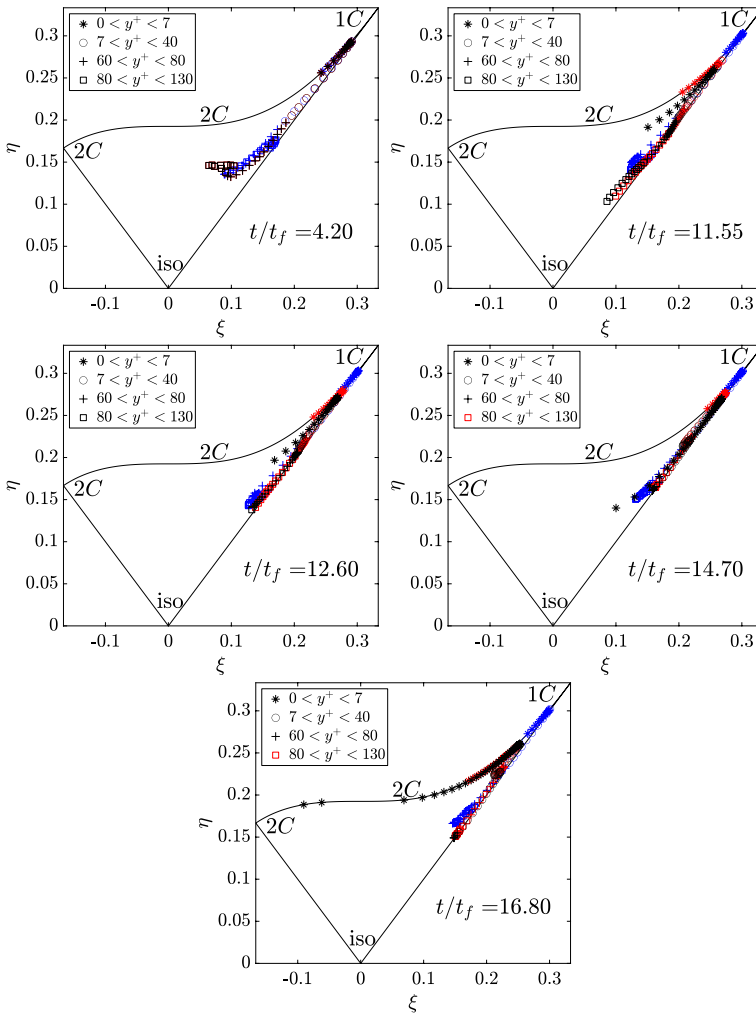


Fig. 30 Lumley triangle on the plane of the invariants η and ξ of the Reynolds stress anisotropy tensor in the turbulent boundary layer HOI configuration with isothermal (red symbols) and adiabatic (black symbols) boundary conditions at different time instants during FWI compared with the non-reacting flow conditions (blue symbols). 1C, 2C and iso imply 1 component limit, 2 component limit and isotropic state respectively

values for both thermal wall boundary conditions, but as the flame propagates towards the wall the Reynolds stresses for $y^+ > 7$ tend towards the one-component limit in the case of isothermal wall and this tendency increases as the flame interacts with the wall, while the Reynolds stresses for $y^+ < 7$ remain at the two component limit as is expected in the non-reacting turbulent boundary layer. In the case of adiabatic wall, during FWI ($t/t_f = 11.55$ and $t/t_f = 12.60$) the trend for $y^+ < 7$ tends to deviate from the non-reacting as well as isothermal wall boundary condition cases as shown in Fig. 30. This variation under adiabatic wall conditions is a consequence of density change until the wall surface as a result of reaction occurring down to the wall surface. At the later stages of FWI (i.e. $t/t_f = 16.80$)

the anisotropy of the Reynolds stresses tend towards the two component limit and this behaviour can be observed for Reynolds stresses up to $y^+ \approx 40$, as shown in Fig. 30. This behaviour of the Reynolds stress anisotropy is more pronounced for the case with adiabatic wall and is expected for both thermal wall boundary conditions, as the flame in this case belongs to the corrugated flamelet regime when it is away from the wall and as in the V-flame OWI cases the integral length scale based on two-point correlation increases towards the wall leading to an even higher Damköhler number. This implies that the flame under these circumstances will introduce a high level of Reynolds stress anisotropy as seen in unconfined statistically stationary planar premixed flames (Ahmed et al. 2019b; Brearley et al. 2019, 2020; Chakraborty 2021).

3.4 Implications on Modelling

The results presented in this work have implications on modelling of turbulence, heat transfer and combustion. It can be inferred from the results for $\overline{\tau}_w$ and \tilde{u}/\tilde{u}_τ profiles for the different wall boundary conditions and flow configurations that near wall turbulence models will need to be updated to account for FWI within turbulent boundary layers. This is especially true in the case of wall functions for velocity and the near wall damping of low Reynolds number formulation of turbulence models used in industrial RANS simulations. The near wall behaviour of temperature and the associated heat transfer models will also need to be modified to account for developing thermal boundary layers encountered during FWI. It should also be noted here that the new models to be developed should also account for the alignment of the mean flame propagation with the wall normal as this has major implications on the flow behaviour as demonstrated in this paper. The data reported in this work can provide a good platform for developing these models, but this is beyond the scope of current work.

4 Summary and Conclusions

Two different turbulent flows in which flames interact with chemically inert isothermal and adiabatic walls at the reactant temperature in fully developed turbulent boundary layers have been investigated by performing direct numerical simulations (DNS). The main difference between the two flow configurations is the flame orientation with respect to the wall during flame-wall interaction (FWI). In the first configuration, oblique flame interaction (OWI) is simulated where a V-flame interacts with the channel wall under different thermal wall boundary conditions, while in the second configuration, head-on interaction (HOI) of a planar flame in a turbulent boundary layer takes place with isothermal and adiabatic walls. Mean quantities such as density, temperature and progress variable have been investigated for both flow configurations under different thermal wall boundary conditions and it is found that these quantities behave in a different manner for the two flame configurations as well as different thermal conditions at the wall. In the case of V-flame OWI, a statistically stationary flame is obtained for both thermal wall conditions while in the case of turbulent boundary layer HOI a transient flame exists and extinguishes due to the heat loss to the wall, under isothermal wall conditions, and also due to the consumption of the fuel within the domain for adiabatic wall condition.

It has been shown that under isothermal wall conditions the quenching distance and the mean wall heat flux to the wall are significantly altered by the choice of the flow

configuration. The flow configuration and different thermal wall conditions also have an effect on the behaviour of the mean wall shear stress and the mean wall friction velocity at the wall. In the case of V-flame OWI, the overall mean wall shear stress increases due to the thermal expansion effects caused by the flame and a local decrease is observed in the region of FWI for both thermal wall boundary conditions, while in the turbulent boundary layer HOI case no overall increase in the mean wall shear stress is observed and a decrease as a consequence of FWI is seen under both isothermal and adiabatic wall boundary conditions. The wall friction velocity tends to follow the same trend as the wall shear stress in both V-flame OWI and turbulent boundary layer HOI cases with isothermal wall conditions, whereas in the cases with adiabatic walls the wall friction velocity tends to increase in the V-flame OWI case with adiabatic walls and tends to stay of the order of unity in the case of boundary layer HOI case with an adiabatic wall. This difference in the wall friction velocity for adiabatic wall boundary conditions when compared with the isothermal wall conditions is caused by the drop in density until the wall surface due to the chemical reaction occurring up to the wall surface. The behaviour of the mean velocity statistics in the log-layer region of the boundary layer is significantly affected by the flame in both flow configurations and under both thermal wall boundary conditions when compared with the corresponding non-reacting flow conditions. Similar trends between the reacting, under both thermal wall boundary conditions, and non-reacting cases have been observed for the mean Reynolds stresses where it is found that the existence of the flames in the near wall region and also during FWI increases the Reynolds stress anisotropy. In the case of V-flame OWI, turbulent kinetic energy is maintained in the near wall region due to the constant supply of turbulence and also due to the shear generated turbulence at the wall caused by thermal expansion effects, while in the case of turbulent boundary layer HOI turbulence kinetic energy decays during FWI as there is no supply of turbulence and the thermal expansion effects are in the wall normal direction which implies that the flow acceleration due to thermal expansion does not generate any shear at the wall. The dissipation rate of turbulent kinetic energy has been found to increase at the wall during FWI in the V-flame OWI configuration, while it decreases in the turbulent boundary layer HOI configuration. This is purely due to the way flames interact with the wall and the way turbulence evolves within the different flow configurations. In both configurations the dissipation rate of turbulent kinetic energy is higher during FWI under adiabatic wall conditions when compared with the dissipation rate of turbulent kinetic energy under isothermal wall conditions.

The fluid-dynamic statistics discussed in this work are unlikely to be affected by the choice of the chemical mechanism as chemistry affects the momentum transport through dilatation rate and density variation. As both density variation and dilatation rate values are adequately captured by single-step chemistry in hydrocarbon-air combustion, the findings of the current analysis will be valid at least in the qualitative sense in the presence of detailed chemistry calculations of premixed turbulent FWI of hydrocarbon fuels. Finally, the findings of the current analysis imply that future model developments of FWI need to account for the relative alignments of flame and wall normal vectors with mean flow direction and thermal boundary conditions for high-fidelity predictions.

Acknowledgements The authors are grateful for the financial support from the Engineering and Physical Sciences Research Council (Grant: EP/P022286/1, EP/V003534/1). The computational support was provided by ARCHER2 (EP/R029369/1, ARCHER2 PR17125), CIRRUS, SuperMUC-NG via Leibniz Supercomputing Centre (Grant: pn69ga, pn34xu), and ROCKET (HPC facility at Newcastle University).

Author Contributions UA conceptualised the analysis, performed the simulations and prepared the original draft. NC and MK reviewed and edited the paper.

Funding This work was supported by the Engineering and Physical Sciences Research Council Grants EP/P022286/1, EP/V003534/1, EP/R029369/1 and ARCHER2 Pioneer Projects. Some of the computational resources were provided by Leibniz Supercomputing Centre Grants: pn69ga and pn34xu.

Declarations

Conflict of interest The authors declare that they have no conflict of interest.

Ethical Approval No specific ethical approval is required for this work.

Informed Consent Not applicable for this work.

Open Access This article is licensed under a Creative Commons Attribution 4.0 International License, which permits use, sharing, adaptation, distribution and reproduction in any medium or format, as long as you give appropriate credit to the original author(s) and the source, provide a link to the Creative Commons licence, and indicate if changes were made. The images or other third party material in this article are included in the article's Creative Commons licence, unless indicated otherwise in a credit line to the material. If material is not included in the article's Creative Commons licence and your intended use is not permitted by statutory regulation or exceeds the permitted use, you will need to obtain permission directly from the copyright holder. To view a copy of this licence, visit <http://creativecommons.org/licenses/by/4.0/>.

References

- Ahmed, U., Doan, N.A.K., Lai, J., Klein, M., Chakraborty, N., Swaminathan, N.: Multiscale analysis of head-on quenching premixed turbulent flames. *Phys. Fluids* **30**(10), 105102 (2018). <https://doi.org/10.1063/1.5047061>
- Ahmed, U., Chakraborty, N., Klein, M.: Insights into the bending effect in premixed turbulent combustion using the flame surface density transport. *Combust. Sci. Technol.* **191**(5–6), 898–920 (2019a). <https://doi.org/10.1080/00102202.2019.1577241>
- Ahmed, U., Chakraborty, N., Klein, M.: On the stress-strain alignment in premixed turbulent flames. *Sci. Rep.* **9**(1), 5092 (2019b). <https://doi.org/10.1038/s41598-019-41599-y>
- Ahmed, U., Pillai, A.L., Chakraborty, N., Kurose, R.: Statistical behavior of turbulent kinetic energy transport in boundary layer flashback of hydrogen-rich premixed combustion. *Phys. Rev. Fluids* **4**(10), 103201 (2019c). <https://doi.org/10.1103/PhysRevFluids.4.103201>
- Ahmed, U., Pillai, A.L., Chakraborty, N., Kurose, R.: Surface density function evolution and the influence of strain rates during turbulent boundary layer flashback of hydrogen-rich premixed combustion. *Phys. Fluids* **32**(5), 055112 (2020). <https://doi.org/10.1063/5.0004850>
- Ahmed, U., Apsley, D.D., Stallard, T., Stansby, P.K., Afgan, I.: Turbulent length scales and budgets of Reynolds stress-transport for open-channel flows; friction Reynolds numbers $Re_{\tau} = 150, 400$ and 1020 . *J. Hydraul. Res.* **59**(1), 36–50 (2021a). <https://doi.org/10.1080/00221686.2020.1729265>
- Ahmed, U., Chakraborty, N., Klein, M.: Assessment of Bray Moss Libby formulation for premixed flame-wall interaction within turbulent boundary layers: influence of flow configuration. *Combust. Flame* **233**, 111575 (2021b). <https://doi.org/10.1016/j.combustflame.2021.111575>
- Ahmed, U., Chakraborty, N., Klein, M.: Influence of thermal wall boundary condition on scalar statistics during flame-wall interaction of premixed combustion in turbulent boundary layers. *Int. J. Heat Fluid Flow* **92**, 108881 (2021c). <https://doi.org/10.1016/j.ijheatfluidflow.2021.108881>
- Ahmed, U., Chakraborty, N., Klein, M.: Scalar gradient and strain rate statistics in oblique premixed flame-wall interaction within turbulent channel flows. *Flow Turbul. Combust.* **106**(2), 701–732 (2021d). <https://doi.org/10.1007/s10494-020-00169-3>
- Ahmed, U., Malkeson, S.P., Pillai, A.L., Chakraborty, N., Kurose, R.: Flame self-interaction during turbulent boundary layer flashback of hydrogen-rich premixed combustion. *Phys. Rev. Fluids* **8**(2), 023202 (2023). <https://doi.org/10.1103/PhysRevFluids.8.023202>
- Alshaaan, T.M., Rutland, C.J.: Turbulence, scalar transport, and reaction rates in flame-wall interaction. *Proc. Combust. Inst.* **27**(1), 793–799 (1998). [https://doi.org/10.1016/S0082-0784\(98\)80474-8](https://doi.org/10.1016/S0082-0784(98)80474-8)
- Alshaaan, T.M., Rutland, C.J.: Wall heat flux in turbulent premixed reacting flow. *Combust. Sci. Technol.* **174**(1), 135–165 (2002). <https://doi.org/10.1080/713712913>

- Aspden, A.J., Day, M.S., Bell, J.B.: Three-dimensional direct numerical simulation of turbulent lean premixed methane combustion with detailed kinetics. *Combust. Flame* **166**, 266–283 (2016). <https://doi.org/10.1016/j.combustflame.2016.01.027>
- Bailey, J., Richardson, E.S.: DNS analysis of boundary layer flashback in turbulent flow with wall-normal pressure gradient. *Proc. Combust. Inst.* **38**(2), 2791–2799 (2021). <https://doi.org/10.1016/j.proci.2020.06.004>
- Brearley, P., Ahmed, U., Chakraborty, N., Lipatnikov, A.N.: Statistical behaviors of conditioned two-point second-order structure functions in turbulent premixed flames in different combustion regimes. *Phys. Fluids* **31**(11), 115109 (2019). <https://doi.org/10.1063/1.5124143>
- Brearley, P., Ahmed, U., Chakraborty, N.: The relation between flame surface area and turbulent burning velocity in statistically planar turbulent stratified flames. *Phys. Fluids* **32**(12), 125111 (2020). <https://doi.org/10.1063/5.0031291>
- Bruneaux, G., Akselvoll, K., Poinso, T.J., Ferziger, J.H.: Flame-wall interaction simulation in a turbulent channel flow. *Combust. Flame* **107**(1–2), 27–36 (1996). [https://doi.org/10.1016/0010-2180\(95\)00263-4](https://doi.org/10.1016/0010-2180(95)00263-4)
- Bruneaux, G., Poinso, T.J., Ferziger, J.H.: Premixed flame-wall interaction in a turbulent channel flow: budget for the flame surface density evolution equation and modelling. *J. Fluid Mech.* **349**, 191–219 (1997). <https://doi.org/10.1017/S0022112097006769>
- Cant, R.S.: Direct numerical simulation of premixed turbulent flames. *Philos. Trans. R. Soc.* **357**, 3583–3604 (1999). <https://doi.org/10.1098/rsta.1999.0511>
- Chakraborty, N.: Influence of thermal expansion on fluid dynamics of turbulent premixed combustion and its modelling implications. *Flow, Turbul. Combust.* **106**(3), 753–848 (2021). <https://doi.org/10.1007/s10494-020-00237-8>
- Chakraborty, N., Katragadda, M., Cant, R.S.: Statistics and modelling of turbulent kinetic energy transport in different regimes of premixed combustion. *Flow, Turbul. Combust.* **87**(2–3), 205–235 (2011). <https://doi.org/10.1007/s10494-010-9312-1>
- Cheng, R.K., Bill, R., Robben, F.: Experimental study of combustion in a turbulent boundary layer. *Symp. Combust.* **18**(1), 1021–1029 (1981). [https://doi.org/10.1016/S0082-0784\(81\)80106-3](https://doi.org/10.1016/S0082-0784(81)80106-3)
- Cheng, R.K., Shepherd, I.: The influence of burner geometry on premixed turbulent flame propagation. *Combust. Flame* **85**(1–2), 7–26 (1991). [https://doi.org/10.1016/0010-2180\(91\)90174-A](https://doi.org/10.1016/0010-2180(91)90174-A)
- Clendening, C.W., Shackleford, W., Hilyard, R.: Raman scattering measurements in a side-wall quench layer. *Symp. Combust.* **18**(1), 1583–1590 (1981). [https://doi.org/10.1016/S0082-0784\(81\)80161-0](https://doi.org/10.1016/S0082-0784(81)80161-0)
- Domingo, P., Vervisch, L., Payet, S., Hauguel, R.: DNS of a premixed turbulent V flame and LES of a ducted flame using a FSD-PDF subgrid scale closure with FPI-tabulated chemistry. *Combust. Flame* **143**(4), 566–586 (2005). <https://doi.org/10.1016/j.combustflame.2005.08.023>
- Dunstan, T.D., Swaminathan, N., Bray, K.N.C., Cant, R.S.: Geometrical properties and turbulent flame speed measurements in stationary premixed V-flames using direct numerical simulation. *Flow, Turbul. Combust.* **87**(2–3), 237–259 (2010). <https://doi.org/10.1007/s10494-010-9284-1>
- Dunstan, T.D., Swaminathan, N., Bray, K.N.C.: Influence of flame geometry on turbulent premixed flame propagation: a DNS investigation. *J. Fluid Mech.* **709**, 191–222 (2012). <https://doi.org/10.1017/jfm.2012.328>
- Ezekoye, O., Greif, R., Sawyer, R.: Increased surface temperature effects on wall heat transfer during unsteady flame quenching. *Symp. Combust.* **24**(1), 1465–1472 (1992). [https://doi.org/10.1016/S0082-0784\(06\)80171-2](https://doi.org/10.1016/S0082-0784(06)80171-2)
- Fernandez-Pello, A.C.: Micropower generation using combustion: Issues and approaches. *Proc. Combust. Inst.* **29**(1), 883–899 (2002). [https://doi.org/10.1016/S1540-7489\(02\)80113-4](https://doi.org/10.1016/S1540-7489(02)80113-4)
- Ghai, S.K., Chakraborty, N., Ahmed, U., Klein, M.: Enstrophy evolution during head-on wall interaction of premixed flames within turbulent boundary layers. *Phys. Fluids* **34**(7), 075124 (2022). <https://doi.org/10.1063/5.0098047>
- Gorski, J.J., Wallace, J.M., Bernard, P.S.: The enstrophy equation budget of bounded turbulent shear flows. *Phys. Fluids* **6**(9), 3197–3199 (1994). <https://doi.org/10.1063/1.868100>
- Gruber, A., Sankaran, R., Hawkes, E.R., Chen, J.H.: Turbulent flame-wall interaction: a direct numerical simulation study. *J. Fluid Mech.* **658**, 5–32 (2010). <https://doi.org/10.1017/S0022112010001278>
- Gruber, A., Chen, J.H., Valiev, D., Law, C.K.: Direct numerical simulation of premixed flame boundary layer flashback in turbulent channel flow. *J. Fluid Mech.* **709**, 516–542 (2012). <https://doi.org/10.1017/jfm.2012.345>
- Gruber, A., Richardson, E.S., Aditya, K., Chen, J.H.: Direct numerical simulations of premixed and stratified flame propagation in turbulent channel flow. *Phys. Rev. Fluids* **3**(11), 110507 (2018). <https://doi.org/10.1103/PhysRevFluids.3.110507>
- Huang, W., Vosen, S., Greif, R.: Heat transfer during laminar flame quenching: effect of fuels. *Proc. Combust. Inst.* **21**(1), 1853–1860 (1988). [https://doi.org/10.1016/S0082-0784\(88\)80420-X](https://doi.org/10.1016/S0082-0784(88)80420-X)

- Jainski, C., Reißmann, M., Böhm, B., Dreizler, A.: Experimental investigation of flame surface density and mean reaction rate during flame-wall interaction. *Proc. Combust. Inst.* **36**(2), 1827–1834 (2017a). <https://doi.org/10.1016/j.proci.2016.07.113>
- Jainski, C., Reißmann, M., Böhm, B., Janicka, J., Dreizler, A.: Sidewall quenching of atmospheric laminar premixed flames studied by laser-based diagnostics. *Combust. Flame* **183**, 271–282 (2017b). <https://doi.org/10.1016/j.combustflame.2017.05.020>
- Jainski, C., Reißmann, M., Jakirlic, S., Böhm, B., Dreizler, A.: Quenching of premixed flames at cold walls: effects on the local flow field. *Flow, Turbul. Combust.* **100**(1), 177–196 (2018). <https://doi.org/10.1007/s10494-017-9836-8>
- Jarosinski, J.: A survey of recent studies on flame extinction. *Prog. Energy Combust. Sci.* **12**(2), 81–116 (1986). [https://doi.org/10.1016/0360-1285\(86\)90014-6](https://doi.org/10.1016/0360-1285(86)90014-6)
- Jenkins, K., Cant, R.: Direct numerical simulation of turbulent flame kernels. In: Knight, D., Sakell, L. (eds.) *Recent Advances in DNS and LES: Proceedings of the Second AFOSR Conference*, Rutgers - The State University of New Jersey, New Brunswick, USA, pp. 191–202. Kluwer, Dordrecht (1999)
- Kays, W.M., Crawford, M.E.: *Convective heat and mass transfer*, 3rd edn. McGraw-Hill, New York (1993)
- Kim, J., Moin, P., Moser, R.D.: Turbulence statistics in fully developed channel flow at low Reynolds number. *J. Fluid Mech.* **177**, 133–166 (1987). <https://doi.org/10.1017/S0022112087000892>
- Kitano, T., Tsuji, T., Kurose, R., Komori, S.: Effect of pressure oscillations on flashback characteristics in a turbulent channel flow. *Energy and Fuels* **29**(10), 6815–6822 (2015). <https://doi.org/10.1021/acs.energyfuels.5b01687>
- Konstantinou, I., Ahmed, U., Chakraborty, N.: Effects of fuel Lewis number on the near-wall dynamics for statistically planar turbulent premixed flames impinging on inert cold walls. *Combust. Sci. Technol.* **193**(2), 235–265 (2021). <https://doi.org/10.1080/00102202.2020.1799201>
- Lai, J., Chakraborty, N.: A priori direct numerical simulation modeling of scalar dissipation rate transport in head-on quenching of turbulent premixed flames. *Combust. Sci. Technol.* **188**(9), 1440–1471 (2016a). <https://doi.org/10.1080/00102202.2016.1195823>
- Lai, J., Chakraborty, N.: Effects of Lewis number on head-on quenching of turbulent premixed flames: a direct numerical simulation analysis. *Flow, Turbul. Combust.* **96**(2), 279–308 (2016b). <https://doi.org/10.1007/s10494-015-9629-x>
- Lai, J., Chakraborty, N., Lipatnikov, A.N.: Statistical behaviour of vorticity and enstrophy transport in head-on quenching of turbulent premixed flames. *Eur. J. Mech. B/Fluids* **65**, 384–397 (2017). <https://doi.org/10.1016/j.euromechflu.2016.10.013>
- Lai, J., Klein, M., Chakraborty, N.: Direct numerical simulation of head-on quenching of statistically planar turbulent premixed methane-air flames using a detailed chemical mechanism. *Flow, Turbul. Combust.* **101**(4), 1073–1091 (2018a). <https://doi.org/10.1007/s10494-018-9907-5>
- Lai, J., Wacks, D.H., Chakraborty, N.: Flow topology distribution in head-on quenching of turbulent premixed flame: a direct numerical simulation analysis. *Fuel* **224**, 186–209 (2018b). <https://doi.org/10.1016/j.fuel.2018.03.021>
- Moser, R.D., Kim, J., Mansour, N.N.: Direct numerical simulation of turbulent channel flow up to $Re_{\tau}=590$. *Phys. Fluids* **11**(4), 943–945 (1999). <https://doi.org/10.1063/1.869966>
- Ng, T., Cheng, R.K., Robben, F., Talbot, L.: Combustion-turbulence interaction in the turbulent boundary layer over a hot surface. *Symp. Combust.* **19**(1), 359–366 (1982). [https://doi.org/10.1016/S0082-0784\(82\)80207-5](https://doi.org/10.1016/S0082-0784(82)80207-5)
- Nishiki, S., Hasegawa, T., Borghi, R., Himeno, R.: Modeling of flame-generated turbulence based on direct numerical simulation databases. *Proc. Combust. Inst.* **29**(2), 2017–2022 (2002). [https://doi.org/10.1016/S1540-7489\(02\)80246-2](https://doi.org/10.1016/S1540-7489(02)80246-2)
- Poinsot, T.J., Haworth, D., Bruneaux, G.: Direct simulation and modeling of flame-wall interaction for premixed turbulent combustion. *Combust. Flame* **95**(1), 118–132 (1993). [https://doi.org/10.1016/0010-2180\(93\)90056-9](https://doi.org/10.1016/0010-2180(93)90056-9)
- Poinsot, T.J., Veynante, D.: *Theoretical and numerical combustion*, 2nd edn. R.T. Edwards, Inc, Philadelphia (2005)
- Pope, S.B.: *Turbulent Flows*. Cambridge University Press, Cambridge (2000)
- Popp, P., Baum, M.: Analysis of wall heat fluxes, reaction mechanisms, and unburnt hydrocarbons during the head-on quenching of a laminar methane flame. *Combust. Flame* **108**(3), 327–348 (1997). [https://doi.org/10.1016/S0010-2180\(96\)00144-7](https://doi.org/10.1016/S0010-2180(96)00144-7)
- Richard, G., Escudié, D.: Turbulence effect on the flame-wall interaction. In: *Int. Symp. Turbul. Shear Flow Phenom.*, pp. 519–523 (1999). <http://www.tsfp-conference.org/proceedings/1999/tsfp1-1999-84.pdf>

- Rimann, M., Jainski, C., Mann, M., Dreizler, A.: Flame-flow interaction in premixed turbulent flames during transient head-on quenching. *Flow, Turbul. Combust.* **98**(4), 1025–1038 (2017). <https://doi.org/10.1007/s10494-016-9795-5>
- Rutland, C.J., Cant, R.S.: Turbulent transport in premixed flames. In: *Proceedings of the Summer Program, Cent. Turbul. Res.*, pp. 75–94. NASA Ames/Stanford University, Palo Alto, California, USA (1994)
- Sellmann, J., Lai, J., Kempf, A.M., Chakraborty, N.: Flame surface density based modelling of head-on quenching of turbulent premixed flames. *Proc. Combust. Inst.* **36**(2), 1817–1825 (2017). <https://doi.org/10.1016/j.proci.2016.07.114>
- Smooke, M.D., Giovangigli, V.: Premixed and nonpremixed test problem results, pp. 29–47. Springer, Berlin Heidelberg (1991)
- Tennekes, H., Lumley, J.L.: *A first course in turbulence*. The MIT Press, Cambridge (1972)
- Tsukahara, T., Seki, Y., Kawamura, H., Tochio, D.: DNS of turbulent channel flow at very low Reynolds numbers. In: *Forth Int. Symp. Turbul. Shear Flow Phenom.*, pp. 935–940. Williamsburg, USA (2005)
- Vosen, S., Greif, R., Westbrook, C.K.: Unsteady heat transfer during laminar flame quenching. *Proc. Combust. Inst.* **20**(1), 75–83 (1985). [https://doi.org/10.1016/S0082-0784\(85\)80490-2](https://doi.org/10.1016/S0082-0784(85)80490-2)
- Wichman, I.S., Bruneaux, G.: Head-on quenching of a premixed flame by a cold wall. *Combust. Flame* **103**(4), 296–310 (1995). [https://doi.org/10.1016/0010-2180\(95\)00100-X](https://doi.org/10.1016/0010-2180(95)00100-X)
- Yoo, C.S., Im, H.G.: Characteristic boundary conditions for simulations of compressible reacting flows with multi-dimensional, viscous and reaction effects. *Combust. Theory Model.* **11**(2), 259–286 (2007). <https://doi.org/10.1080/13647830600898995>
- Zhang, S., Rutland, C.J.: Premixed flame effects on turbulence and pressure-related terms. *Combust. Flame* **102**(4), 447–461 (1995). [https://doi.org/10.1016/0010-2180\(95\)00036-6](https://doi.org/10.1016/0010-2180(95)00036-6)
- Zhao, P., Wang, L., Chakraborty, N.: Analysis of the flame-wall interaction in premixed turbulent combustion. *J. Fluid Mech.* **848**, 193–218 (2018a). <https://doi.org/10.1017/jfm.2018.356>
- Zhao, P., Wang, L., Chakraborty, N.: Strain rate and flame orientation statistics in the near-wall region for turbulent flame-wall interaction. *Combust. Theory Model.* **22**(5), 921–938 (2018b). <https://doi.org/10.1080/13647830.2018.1465598>
- Zhao, P., Wang, L., Chakraborty, N.: Vectorial structure of the near-wall premixed flame. *Phys. Rev. Fluids* **4**(6), 1–16 (2019). <https://doi.org/10.1103/PhysRevFluids.4.063203>